Magnetospheric Multiscale Mission (MMS): Extended Mission

T.E. Moore, MMS Project Scientist • J.L. Burch, MMS-SMART PI

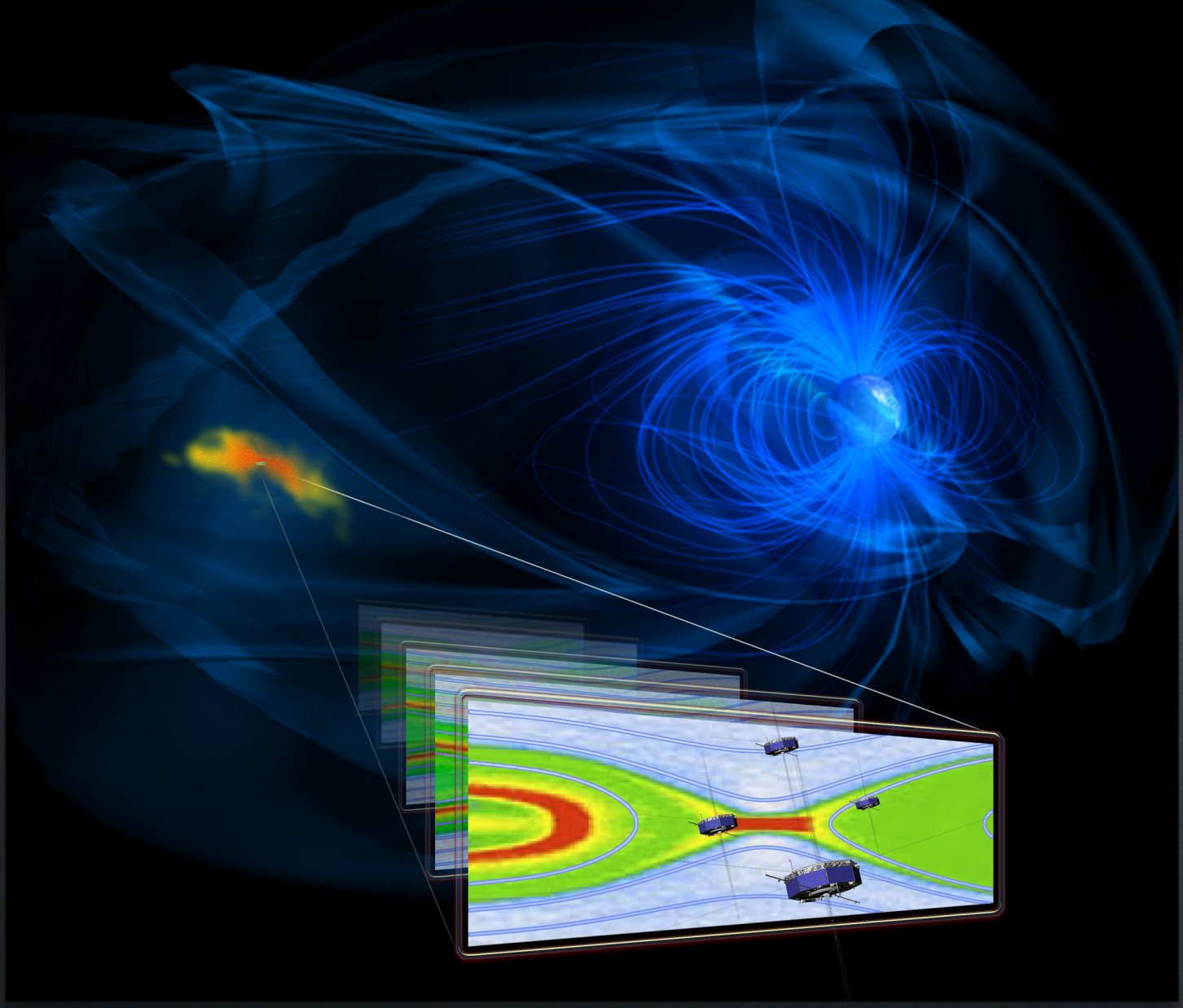

Submitted to the Senior Review 2017 of the Mission Operations and Data Analysis Program for the Heliophysics Operating Missions

MMS

Magnetospheric Multiscale Mission

T. E. Moore, MMS Project Scientist
J. L. Burch, MMS-SMART P.I.

Table of Contents

1.0 Executive Summary

MMS has the overall objective of investigating magnetic reconnection in the boundary regions of the Earth's magnetosphere. The MMS science mission commenced on Sept. 1, 2015 after six months of instrument commissioning. The prime mission is conducted in two phases—Phase 1 on magnetopause reconnection and Phase 2 on magnetotail reconnection. During Phase 1, which ended on February 9, 2017, MMS made many fundamental discoveries about reconnection at the dayside magnetopause. Reconnection was also discovered within Kelvin-Helmholtz events along the post-dusk magnetopause and within flux transfer events (FTEs). In addition to these reconnection results, MMS discovered fundamental properties of bursty bulk flows and other injection events in the near tail region. As a result of the 12 R_E dayside apogee, over 300 bow shock events were captured with burst-mode data, which have revealed electron-scale interactions leading to numerous publications on newly discovered shock phenomena such as whistler-wave electron acceleration and magnetic-field dissipation.

Because of the unprecedented speed and accuracy of the MMS measurements and the close spacing of the spacecraft, experimental results on magnetic reconnection in space have now exceeded the scope of contemporary theory and modeling results. At the same time several predictions from plasma simulations of reconnection have been confirmed, for example, the crescent-shape electron distributions that carry the out-of-plane current near the electron stagnation region (Chen et al., 2016a,b; predicted by Hesse et al., 2014). Further interplay between modeling and experiment are moving our understanding of magnetic reconnection forward at an unprecedented rate. MMS has identified the plasma distribution functions and electric fields responsible for the dissipation of magnetic energy and the breaking and reconnection of magnetic field lines from the Earth and the Sun (Burch et al., 2016). Further studies have demonstrated the dependence of these phenomena on the reconnection guide field (out-of-plane magnetic field), which when moderate to strong provides a channel for out-of-plane current near the magnetic null that is comparable to that provided by the meandering crescent electrons at the stagnation point (Burch and Phan, 2016; predicted by Hesse et al., 2016). Plasma wave generation by beam-plasma interactions within the Electron Diffusion Region (EDR) has been discovered (Graham et al., 2016) and attributed to the crescent-shaped electron distributions.

During the extended mission MMS has 4 Prioritized Science Goals (PSGs): (1) Investigate magnetic reconnection in all near-Earth environments, (2) determine the processes which heat plasma populations and accelerate particles to large energies, (3) study the way turbulent processes interact on kinetic scales, and (4) investigate the microphysics of collisionless shocks.

The results to date from the prime mission have been reported in 58 papers in a special issue of GRL, two papers in both Science and Nature, 5 papers in Phys. Rev. Letters, 3 in JGR and 10 additional papers in GRL. A special issue of JGR is now in preparation.

At the end of Phase 2 (in September 2017) similar advances are expected for magnetotail reconnection, which has symmetric inflow conditions as opposed to the asymmetric conditions that prevail at the magnetopause. In the extended mission, lessons learned from Phases 1 and 2 will be used to implement optimum tetrahedron sizes while modifying the on-board burst quality indices to increase the number of reconnection events that are captured. In addition, the dayside 25 R_E apogee orbit provides opportunities for extending the understanding of reconnection into parameter regimes, such as in solar wind reconnection, that were either poorly sampled or not sampled at all in the prime mission. The unprecedented plasma and field measurements and the tight tetrahedron formation will also be used to make advances in the physics of solar-wind turbulence, particle acceleration, and interplanetary shocks. Finally, the second tail pass will provide downstream magnetopause encounters with Kelvin-Helmholtz events. This region will be missed in Phase 2a because of limitations on science operations during the apogee raise.

An important enabler of the success of the prime mission has been the Scientist-in-the-Loop (SITL) function, in which each day a dedicated MMS scientist examines summary data to identify important events and either add these to the events selected by the on-board burst-monitor system or change the priorities of the selected events. This function is crucial because only about 5% of the acquired burst-mode data can be sent to the ground. The SITL function has proven to be an important supplement to

the on-board system and will be continued through the extended mission. About 25 scientists have been trained as SITLs and their effectiveness depends on their active involvement in analysis of the MMS data.

During the extended mission MMS has 4 Prioritized Science Goals (PSGs): (1) investigate magnetic reconnection in all near-Earth environments, (2) determine the processes which heat plasma populations and accelerate particles to large energies, (3) study the way turbulent processes interact on kinetic scales, and (4) investigate the microphysics of collisionless shocks. The four prioritized science goals are accomplished in four campaigns during each year of the extended mission (Fig. 1-1, Table 5.2-1). Campaigns A and B are on the dayside, post- and pre-noon, respectively, with Campaign A starting at the duskside downstream magnetopause. Campaign C covers the downstream magnetopause on the dawn side, and Campaign D covers the magnetotail.

Since March 2016 MMS has a completely open data set. Level 2 data are posted on the public site within 30 days of data acquisition. All data are in CDF format, which can be read and plotted with various software packages such as IDL, Python, Matlab, and Autoplot. In addition, MMS maintains a comprehensive software package known as SPEDAS (Space Environment Data Analysis System), which is inherited from the THEMIS program but which has specific procedures for MMS. As a result of the easy public data access and the existence and maintenance of SPEDAS, MMS data are widely used throughout the international heliophysics community.

All four MMS spacecraft are 100% healthy as are nearly all of the 100 instruments. The exceptions are one of two EDIs on MMS2, which is limited to ambient mode, the limitation of the EIS on MMS1 to electron measurements only, and a reduction of accuracy of SDP electric field measurements due to a micrometeorite impact. The flexible operations plan that is used in the primary mission and the combination of high time resolution and tight tetrahedral formations are keys to the extraordinary successes of the MMS mission. The uniqueness of the MMS data and the amazing potential for future discoveries are assured when this operations plan is carried into the extended mission without significant modification. The mission has finite fuel reserves that will likely allow maintenance of the tetrahedron throughout the extended mission. Therefore, with the proven operations plan and full funding requested in this proposal, MMS will continue to make discoveries and expand the understanding of reconnection, particle acceleration, and turbulence.

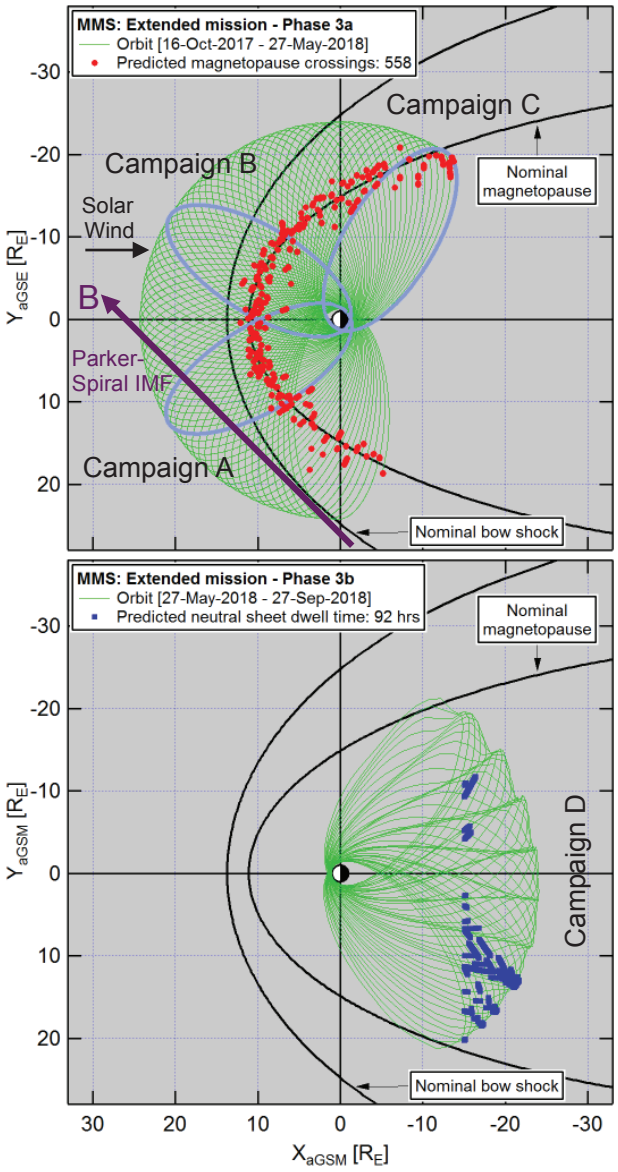

Figure 1-1. MMS orbits (in green) projected into the X-Y GSE (top) and GSM (bottom) planes for the first year of the extended mission. Each year is divided into two phases, a dayside phase (3a, 4a, etc.) and a nightside phase (3b, 4b, etc.). The spacecraft locations during these phases enable four distinct campaigns with new science foci, in addition to extending the magnetopause and magnetotail science that was conducted during the prime mission.

Science and Science Implementation

2.0 The First Phase of the MMS Prime Mission: Scientific Accomplishments

The MMS investigation of magnetic reconnection at the dayside magnetopause began on 1 September 2015 and concluded on 9 February 2017 with the beginning of a series of maneuvers to raise apogee to 25 R_E in preparation for the magnetotail phase. During the dayside phase of the mission, MMS made transformational observations of the kinetic structures of diffusion regions during magnetopause reconnection. The two orders of magnitude higher cadence on 3D electron distribution functions (DFs) and 20 times higher time resolution on ion DFs than previously possible have proven to be crucial in revealing the key particle dynamics and energy conversion in and around the electron and ion diffusion regions. MMS also made several important discoveries regarding the role of turbulence in the dynamics of magnetic reconnection and the still poorly understood nature of flux transfer events. In addition, MMS provided the first definitive observations of reconnection occurring in a Kelvin-Helmholtz vortex along the magnetosphere's dusk flank. During the first year of operation, MMS-based research has led to more than 120 refereed publications containing an exceptionally large amount of new knowledge, a proper report of which is impossible to present here. Instead, some key results are highlighted below, and some additional results are listed in Table 2-1. A link to the complete list of publications is given in §3.1.

2.1 Reconnection at the Dayside Magnetopause and in the Magnetosheath

2.1.1 Electron microphysics. Burch et al. [2016] and Chen et al. [2016b] reported the first detection of the electron diffusion region (EDR) at the dayside magnetopause for small guide field. Electron acceleration and demagnetization were deduced from the unprecedented observation of non-gyrotropic crescent-shaped electron velocity-space distributions (Fig. 2.1-1), which were predicted by simulation [Hesse et al., 2014]. The crescent distribution is due to meandering magnetosheath electrons crossing a thin current sheet, and the crescent shape is caused by sub-gyro-scale sampling of the electrons accelerated by the normal electric field and the reconnection electric field. In the EDR the J dot E dissipation was enhanced. Burch et al. [2016] also observed the mono-directional diversion of the crescent distributions along the magnetic field, which was interpreted as the first direct detection of the opening of a magnetic field line.

Burch and Phan [2016] extended these measurements to the case of a moderate guide field and found that near the flow stagnation point, the crescent-shaped distributions were again observed, but near the x-line (where for small guide field very small currents were observed) strong currents were observed to be carried by field-aligned electron beams. Hesse et al. [2016] extended the simulation work to investigate moderate guide fields and found crescent distributions at the flow stagnation point and field-aligned beams at the x-line, as had been observed by MMS. They also found that the reconnection electric field is produced by electron inertia effects at the x-line and by divergence of the electron pressure tensor at the stagnation point.

Torbert et al. [2016] examined the contributions of electron bulk inertia and pressure divergence to the reconnection electric field for small guide field and found contributions from both effects that nevertheless fell short of balancing the electric field. It was argued that the electron effects may have been underestimated owing to the 10 km (~5 electron skin

Table 2-1 Additional results from the first phase of the MMS prime mission

Energetic particle escape	Mauk et al. 2016; Burch et al. 2016; Cohen et al. 2016; Nagai et al. 2016; Westlake et al. 2016; Lee et al. 2016; Jaynes et al. 2016
Location of reconnection x-line	Trattner et al. 2016; Petrinec et al. 2016; Gomez et al. 2016; Fuselier et al. 2016; Kitamura et al. 2016
Magnetopause location and motion associated with high-latitude dynamics	Le et al. 2016; Anderson et al. 2016
Rippled bow shock	Johlander et al. 2016
Electron acceleration at the bow shock	Oka et al. 2016
Magnetotail flow braking regions	Schmid et al. 2016; Breuillard et al. 2016; Gershman et al. 2016; Goodrich et al. 2016
Substorm/storm time dipolarization	Nakamura et al. 2016; Reiff et al. 2016; Turner et al. 2016; Baker et al. 2016; Matsui et al. 2016
Energetic electron injections	Fennell et al. 2016

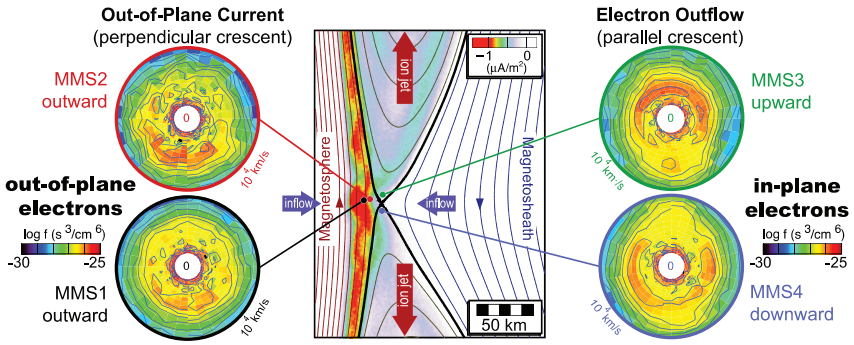

Figure 2.1-1. Nongyrotropic electron distributions observed inside the electron diffusion region, together with a simulation tailored to the event under study. The figure demonstrates the unprecedented quality of electron measurements, and the benefit of a synergistic approach, which combines MMS observations with concurrent modeling. [Burch et al., 2016].

depths) spacecraft separation being too large. To improve on the quantitative evaluation of the electron effect, the spacecraft separation was reduced to 7 km for Phase 1b. This reassessment of the separation is an excellent example of the flexible mission operations based on lessons learned in previous mission phases.

Non-gyrotropic crescent-shape electron distributions were also seen along the separatrices slightly downstream of the x-line [Norgren et al., 2016; Phan et al., 2016], indicating that electron dynamics operating in the electron diffusion region extends some distance downstream of the x-line, in agreement with simulation [Bessho et al., 2016; Shay et al., 2016; Chen et al., 2016b].

The high time resolution of FPI electron measurements allowed Lavraud et al., [2016] to resolve inflowing, outflowing and bouncing populations within a reconnecting current sheet. Close separation of the MMS spacecraft permitted the identification of a region of strongly curved magnetic field, where low-energy electrons are scattered. Electron heating in a region with strong lower-hybrid drift (LHD) turbulence and related electron-scale currents was reported by Graham et al. [2016]. They concluded that the heating is consistent with trapping by parallel electric fields rather than wave-particle interactions, based on the spatial separation between the heating and wave power peaks. MMS also provided the first identification of electron-scale super-Alfvénic reconnection outflow jets [Khotyaintsev et al., 2016; Norgren et al., 2016; Phan et al. 2016] and the associated $E_{\parallel}$ fluctuations driven by the Buneman instability [Khotyaintsev et al., 2016]. Fast electron measurements by EDI and FPI indicated that the instability leads to thermalization and braking of the electron jet.

At the magnetospheric separatrix of the reconnecting magnetopause, MMS discovered substantial parallel electron acceleration by time domain structures (TDS), which are millisecond duration pulses of parallel electric field that move along the magnetic field line [Mozer et al., 2016]. Two MMS spacecraft observed TDS traveling away from the x-line along the magnetic field at 4000 km/sec, accelerating field-aligned ~5 eV electrons to ~200 eV by a single Fermi reflection of the electrons by these overtaking barriers. Such a fast and strong acceleration process (corresponding to a factor of ~40 energy increase) may be one important new component in the chain of phenomena associated with reconnection and leading to global plasma heating.

With the unprecedented capability of accurately measuring current density at 30 ms resolution using plasma measurements, MMS revealed the abundant presence of electron-scale filamentary Hall currents and electron vorticity within the reconnection exhaust far downstream of the x-line, in the region where one would have expected the plasma to be frozen-in (i.e., MHD-like) [Phan et al., 2016].

2.1.2 Ion microphysics. FPI's fast ion measurements provided important new insights into ion dynamics related to reconnection, clearly demonstrating in particular the intrusion of magnetosheath ions into the magnetospheric inflow [Khotyaintsev et al., 2016; Burch and Phan, 2016]. Owing to its equatorial orbit, MMS frequently encounters regions populated by cold ions of plasmaspheric origin. MMS thus succeeded in quantitatively verifying earlier Cluster results suggesting that such ions introduce a new length scale and modify the Hall physics of magnetic reconnection [André et al., 2016]. High-resolution observations of cold ions near the x-line revealed a sub-region within the ion diffusion region, where the cold ions are demagnetized and accelerated parallel to the Hall electric field.

Demagnetized magnetosheath ions near the current sheet mid-plane with Speiser-type motion are observed close to the X-line with signatures of ac-

celeration by the reconnection electric field and gyro-turning to form the outflows [Wang et al., 2016a]. Ion demagnetization also occurs tens of ion skin depths downstream from the x-line but shows no signatures of acceleration by the reconnection electric field and gyro-turning [Wang et al., 2016b].

2.1.3 Waves and turbulence. The magnetospheric separatrix close to the EDR is observed to be associated with tangled, reconnected magnetic fields [Ergun et al., 2016a] and may be involved in secondary reconnection. The results provide the first direct measurements to indicate turbulent reconnection along the separatrix layers. Ergun et al. [2016a] also showed that double layers associated with twisted magnetic flux ropes were often found near the diffusion region on the separatrix, and suggested that they were an indication that magnetopause reconnection is either patchy or turbulent. Price et al. [2016] showed that turbulence developed near both the x-line and the separatrices when PIC simulations of reconnection were extended to three dimensions, and that non-gyrotropic crescent electron distributions persisted even during turbulent reconnection. MMS also made progress in understanding the role of wave phenomena associated with reconnection. For example, the separatrix was shown to be a source for the emission of whistler waves that propagate towards the x-line [Le Contel et al., 2016]. The parallel electric field of these waves was shown to be non-linear and is potentially associated with localized "bunching" of electrons on the order of a few electron skin depths, as well as a resonant interaction with an electron beam [Wilder et al., 2016a]. Further, Zhou et al. [2016] showed that the ion diffusion region was a source for electrostatic waves, including electron cyclotron harmonics on the magnetosheath separatrix, and a beam mode on the magnetospheric separatrix. Finally, it was shown that at the dayside magnetopause, cold magnetospheric electrons near the diffusion region interacted with incoming magnetosheath electrons leading to very large amplitude (~100 mV/m) oscillations in the parallel electric field, potentially with a net electrostatic potential drop [Ergun et al., 2016b].

MMS data have enabled detailed studies of kinetic-scale plasma processes in the turbulent magnetosheath environment. Small spacecraft separation allowed determination of magnetosheath turbulence properties in the ion-kinetic range for the first time using the wave telescope technique [Narita et al., 2016]. An ion-scale magnetic island was studied in detail by Huang et al. [2016], and electron beams and intense wave emissions in the island could be resolved using the novel MMS capabilities. MMS also enabled detection of ion demagnetization, electron jets, electron heating, and nongyrotropy within electron-scale structures in turbulent magnetosheath, which suggests ongoing reconnection [Yordanova et al., 2016]. A strong ion-scale current sheet forming at a magnetosheath jet was reported by Eriksson et al. [2016], who detected local field-aligned acceleration of electrons and attributed it to shock-like acceleration. MMS also allows the study of reconnection at scales significantly larger than the electron and ion scales. Magnetosheath observation of a burst of energetic (50–1000 keV) proton, helium, and oxygen ions exhibiting an inverse dispersion could be attributed to the leakage along reconnected field lines of betatron-accelerated energetic ions (Lee at al., 2016).

2.1.4 Flux transfer events and flux ropes. A common feature of in situ observations at the magnetopause are flux transfer events (FTEs), characterized by bi-polar variation in the component of the magnetic field normal to the magnetopause. FTEs are results of reconnection processes at the magnetopause. Many FTEs are found to have a flux rope structure, with helical magnetic fields wound about a strand of core flux. Although typically created by reconnection, several different scenarios have been proposed for their formation. A deeper understanding of FTEs/flux ropes, the role they play in magnetopause reconnection, and their impact on magnetospheric dynamics requires the high-time resolution multipoint measurements, which can only be provided by MMS.

Research with this data set has led to a number of discoveries. Eastwood et al. [2016] showed that flux ropes exist down to ion scales (this population has not been resolved by previous space missions) and that they can be produced by secondary instabilities. Øieroset et al. [2016] found that compressed thin current sheets can form inside a magnetic flux rope as a result of converging flows and that these current sheets themselves can re-reconnect. Farrugia et al. [2016] showed further that flux ropes do not necessarily exhibit a force-free structure, which explains the plasma motion in and around the FTE as well as their motion along the magnetopause. Mesoscale flux transfer events decay as the reconnection jet evolves with distance from the x-line as demonstrated by Hasegawa et al. [2016]. Hwang et al. [2016]

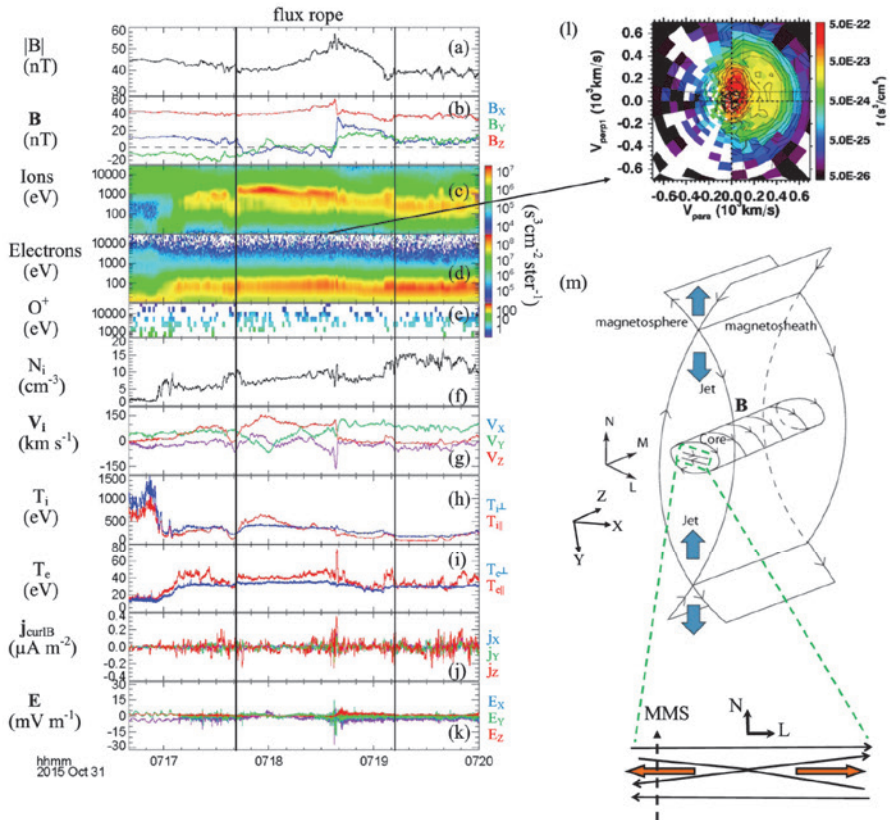

Figure 2.1-2. MMS4 flux rope observations in GSE coordinates. The panels on the left show MMS observations: (a) magnetic field magnitude, (b) magnetic field components, (c) ion energy spectrogram, (d) electron spectrogram, (e) O^+ counts, (f) ion density, (g) ion velocity, (h) ion temperature, (i) electron temperature, (j) current from plasma measurement, and (k) electric field. The panels on the right show (l) a 2-D cut of the ion distribution at the indicated time and (m) a simplified cartoon of the location of a thin current sheet inside a flux rope, as well as the inferred MMS trajectory across the reconnection layer. These observations show that symmetric reconnection can occur between colliding electron jets. [Øieroset et al., 2016].

demonstrated that the magnetic field inside an FTE exhibits extremely complex and time-varying connectivity, which is important for understanding their topology and role in transporting flux into the magnetosphere.

2.1.5 Reconnection in Kelvin-Helmholtz Vortices. Certain directions of the ambient magnetic field in a plasma flow shear allow the Kelvin-Helmholtz (KH) instability to grow and form magnetopause surface waves along the Earth's magnetopause flanks. The surface wave dynamics may compress the magnetopause current sheet, and eventually allow it to roll up into vortices farther down the flanks. Many reports, prior to the launch of MMS, proposed that KH-related current sheets should be able to support a local onset of magnetic reconnection, sustain reconnection exhausts, and even form magnetic flux ropes. However, these current sheets typically propagate at a good fraction of the 200-300 km/s magnetosheath flow speed, making it nearly impossible to confirm the various signatures of reconnection using classical particle instrumentation techniques with multi-second measurement cadences.

Eriksson et al. [2016] reported the first direct evidence of reconnection for a large fraction of compressed KH-related current sheets. They also reported asymmetric Hall magnetic and electric fields consistent with a strong guide-field and a weak density asymmetry. Li et al. [2016] found new evidence for field-aligned heating of magnetosheath electrons and a gradual ion mixing associated with KH-related reconnection jets. Vernisse et al. [2016] discovered that a majority of these exhausts were consistent with a leakage of magnetospheric electrons into the adjacent magnetosheath in agreement with an open field topology. They also reported electron signatures that suggest a more complex 3-D topology with reconnection sites at higher latitudes. Wilder et al. [2016b] reported the presence of large-amplitude electrostatic waves within a Kelvin-Helmholtz vortex and proposed that the presence of cold electrons promoted this wave growth. Stawarz et al. [2016] found the first evidence of plasma turbulence signatures within KH-waves in their early stages of evolution that required the high-time plasma resolution of the MMS.

2.2 Further Scientific Successes with MMS

Although the focus of the MMS mission is on reconnection microphysics, the dayside phase of the mission has also provided significant new results on

a number of other topics, including the large-scale structure and dynamics of magnetopause reconnection, the escape of energetic particles across the magnetopause, and electron acceleration at the bow shock. In addition, during the commissioning phase and Phase 1x, MMS crossed the near-Earth magnetotail at radial distance up to 12 R_E. Although they are not prime science phases, the unprecedented high time resolution data from the four spacecraft separated at distances less than the proton gyro-scale enabled new observations of sub-ion scale signatures in the plasma sheet. These signatures are associated with the braking of bursty bulk flows (BBF) and dipolarization fronts, which play an important role in the dissipation processes of the energy transferred from the magnetotail reconnection region. The observations offered a preview of processes to be explored in depth during the magnetotail phase of the prime mission, to begin in late May/early June of 2017. Some representative results are summarized in Table 2-1.

3.0 Productivity and Impact

3.1 Productivity and Vitality

Even at this relatively early stage, the MMS mission has been exceptionally productive. Since the beginning of the prime science mission, MMS results have been reported in 58 papers in a special issue of GRL, two papers in both Science and Nature, 5 papers in Phys. Rev. Letters, 3 in JGR, and 10 additional papers in GRL. A special issue of JGR is now in preparation. MMS results from the first phase of the mission and related theory and modeling papers were also heavily represented at the Fall meetings of the American Geophysical Union, with 93 oral presentations and posters at the 2015 meeting and 125 at the 2016 Fall meeting. MMS results have been presented at the 2016 European Geophysical Union as well at various topical meetings and workshops such as the US-Japan Workshop on Magnetic Reconnection and the 4th Cluster-THEMIS Workshop. The MMS team engaged the broader heliophysics community at the first MMS Science Community Workshop held at UCLA in September 2016; a second community workshop is planned for June 2017. Lists of MMS publications and conference presentations can be accessed at: https://lasp.colorado.edu/mms/sdc/

In addition to its senior members, the MMS team comprises mid-career and early career/young scientists as well as post-doctoral scientists and graduate students. The team's broad age distribution provides for the mentoring of scientists at the early stages of their careers and ensures the continued availability of the expertise and corporate knowledge required for the calibration, validation and archiving of the wealth of MMS data to be obtained during the extended mission.

22 graduate students, 13 post-docs, and 8 early career/young scientists are currently working on MMS data. 7 Ph.Ds have been awarded for research using MMS data.

3.2 Promise of Future Impact

The MMS mission is a unique, high precision, microscope, which is designed to investigate key microscopic plasma processes that shape our space environment. Owing to this uniqueness alone, MMS is virtually guaranteed to produce otherwise inaccessible scientific information and insight. However, the science activities proposed here are carefully selected to focus on key challenges within NASA's overall quest to understand the space environment, the processes that shape its structure and dynamics, and the processes behind harmful space weather effects. Furthermore, these science topics find broad applications in solar plasmas, and outside of heliophysics, in astrophysics, and even in laboratory plasmas. Finally, the broad and rapid accessibility of MMS data products will continue to enable broad participation of the science community beyond the MMS science team, which has so far provided, and will continue to provide, outstanding scientific productivity.

4.0 Data Accessibility

The MMS team has held as a tenet that maximizing scientific output requires including the provision of rapid access to science quality data products combined with tools to perform advanced analysis of these data sets. The team has therefore established, early on, a strategic thrust designed to provide these services, not only for the MMS science team, but for the broad international science community. As evidenced by the exceptional scientific productivity enabled by the MMS mission, which also includes extensive research conducted outside the MMS team or in conjunction with other components of the HSO, this goal has been met with extraordinary success. The following is a description of these services.

Table 4-1 Quick Facts about MMS Data at the SDC	
Data Storage	60 terabytes (TB) as of 1 Jan 2017
Data Increase	Average of 250 GB per day generated by ~1500 SDC processing jobs
Community Access	~1 TB per day, ~3100 page views per day, served to users in 17 countries
Availability	Since March 2016 all data available within 30 days of receipt at: https://lasp.colorado.edu/mms/sdc/public/

The MMS Science Data Center (SDC) at LASP serves as the central hub for MMS data related activities, including processing, archiving, visualization, and distribution (see Table 4-1). All MMS data levels are managed by the SDC and are disseminated both within and external to the MMS team in the most effective ways possible. Raw data from the Payload Operations Center (POC) are automatically ingested into the SDC and made available to the instrument teams along with the necessary ancillary data, for inspection, analysis, and processing into higher-level data products. A central responsibility of the SDC is to provide a robust, scalable processing environment in which the Instrument Team Facilities (ITFs) produce Level 1 and Level 2 data products within a controlled environment and within the fastest possible time.

The SDC further provides an array of web services that provide data access tools supporting multiple platforms and methods. These web services provide interfaces that can be used from a web browser, used on a command-line, or accessed via scripts or other software, and are intended to maximize versatility. An additional set of features on the SDC website are selected MMS data visualizations. These include visualizations of the spacecraft in their orbit around Earth, the changing structure of their formation, and QuickLook plots that are generated by the SDC and serve as the first glimpse of the returned data. The SDC creates and publishes forty-one unique QuickLook plots daily at a variety of temporal resolutions.

MMS data are stored in Common Data Format (CDF) files, which are extensively self-documenting to SPASE standards. Their contents are fully documented by an online data products guide linked to the above front page of the public MMS Science Data Center under the menu item "About the Data": https://lasp.colorado.edu/mms/sdc/public/about/, which links to detailed pages for each of the MMS instruments: ASPOC, EPD, FIELDS, FPI, and HPCA, as well as other resources such as directories available for browsing, web services documentation, and a data search engine. Data processing status tools are also linked from this page. Each instrument's data products page provides links to both a downloadable, searchable PDF document, and to a set of web page spreadsheets that fully enumerate and describe the data products available for each instrument in the CDF files.

All data within the SDC are continually backed up both on-site and off-site (using Amazon's Glacier service) to provide recovery in the case of system failure. The designated final archive for the MMS mission is the Space Physics Data Facility (SPDF), which also receives many of the MMS science products on an ongoing basis. The SPDF uses the web services developed at the SDC to transfer and archive daily the MMS data files created at the SDC, keeping their archive up to date with the SDC. Similarly, several MMS science team groups have established their own data mirrors at their home institutions and run daily updates to provide local access to the latest data versions for team use.

The MMS team has collaborated with the THEMIS team to provide software data analysis tools based on the Interactive Data Language interpreter, known as the Space Physics Environment Data Analysis Software (SPEDAS), which facilitates direct access to all MMS Level 2 data products by anyone with the necessary tools and skills. SPEDAS is fully documented online at sites that are readily searched online (e.g., http://spedas.org). Training sessions on the use of SPEDAS with MMS data are regularly held at AGU meetings and MMS Community Data Analysis Workshops. MMS Level 2 CDF files are also accessed using a number of inexpensive or freeware tools, for example Autoplot, by those who do not have IDL licenses.

5.0 Extended Mission Science Plan

5.1 Relevance to NASA's Heliophysics Science Goals

NASA's Heliophysics goals, as described in the 2014 SMD strategic plan, are:

G1: Explore the physical processes in the space environment from the Sun to the Earth and throughout the solar system

G2: Advance our understanding of the connections that link the Sun, the Earth, planetary space environments, and the outer reaches of the solar system

G3: Develop the knowledge and capability to

detect and predict extreme conditions in space to protect life and society and to safeguard human and robotic explorers beyond Earth.

As a mission that studies the fundamental plasma process of magnetic reconnection, MMS has addressed and will continue to address in the extended mission all of G1-G3. In addition to its fundamental nature as a space plasma process, magnetic reconnection also facilitates the energetic and transport linkage between different heliophysics domains. Finally, it is the process that underlies the energy conversion necessary to power space weather – the quantitative understanding of which is of key importance for precise space weather forecasting models.

Beyond reconnection, the prioritized science goals of the extended mission also address directly, or indirectly, one or more of NASA's goals in heliophysics. NASA's goals G1-G3 are referenced, as appropriate, for each prioritized science target in this proposal.

The extended mission offers excellent opportunities to improve on the statistics of electron diffusion region (EDR) encounters and investigate important aspects of particle acceleration, reconnection, and turbulence that were not possible or were limited in the prime mission.

5.2 Extended Mission Implementation

5.2.1 MMS Orbit and Constellation in the Extended Mission. At the end of the prime mission (Phase 2b), MMS will be in a 25 R_E apogee, nominally 28º inclination orbit with apogee on the dusk terminator (at 1800 LT). The constellation will be in a tetrahedral configuration with inter-spacecraft spacing at the optimum distance for magnetotail reconnection studies. At the start of the extended mission, the inter-spacecraft spacing is decreased to 30 km (if it is not already at that spacing) or lower, if navigation permits to prepare for the dayside phase. The orbit precesses around in local time so that the apogee is back on the dusk side terminator after approximately one year. In each year in the extended mission, there are 2 phases, a dayside phase (3a, 4a, 5a, etc.) and a tail phase (3b, 4b, 5b, etc.). Fig. 1-1 shows the orbit configurations for Phases 3a and 3b, the first year of the extended mission. Early in the second year of the extended mission, i.e., in Phase 4a, the apogee will be raised to 28 R_E (for disposal purposes at the end of mission). Thereafter, no more maneuvers are performed to change the orbit.

The spacecraft are maintained in a tetrahedron configuration with inter-spacecraft separation for the dayside phases (3a, 4a, etc.) nominally at 30 km. For the tail phases (3b, 4b, etc.), the separation is nominally at the optimum separation determined in August/September 2017 during Phase 2b of the prime mission. The close tetrahedron configuration is planned to be maintained in the extended mission to at least October 2021 and probably to January 2023. Thereafter, the configuration will evolve into a string-of-pearls geometry.

5.2.2. MMS Extended Mission Campaigns. The precession of the MMS orbit creates opportunities to improve the statistics of Electron Diffusion Region encounters at the magnetopause and in the magnetotail and to validate previously obtained understanding. A total of 558 complete magnetopause crossings is predicted for Phase 3a, adding to the more than 6000 partial and complete crossings obtained in the prime mission. In Phase 3b, the spacecraft spend a total of 92 hours within 0.5 R_E of the tail neutral sheet. This time is added to the nearly 300 hours that MMS will spend near the tail neutral sheet in Phase 2b of the prime mission. The extended mission goes far beyond a continuation of reconnection research from the prime mission and the addition of reconnection events. Instead, the orbits enable exploration of other regions of near-Earth space where particle acceleration, reconnection, and turbulence are occurring. The orbit precession in the extended mission divides the dayside and nightside phases into four distinct campaigns (labeled A through D in Fig. 1-1) where new physics is investigated using the unique capabilities of MMS. All campaigns provide broad opportunities to study aspects of the prioritized science goals, with special emphasis described in the following.

In Campaign A, the spacecraft spend a significant amount of time upstream from the Earth's bow shock in the solar wind. Because the average IMF is in the Parker spiral orientation, as shown in Fig. 1-1 (top

Table 5.2-1 MMS campaigns during the extended mission

Campaign	Spacecraft Location	PSGs addressed
A	Duskside bow shock, solar wind, and dusk flank magnetopause	1.2, 1.3, 2.1, 3.1, 3.2 3.3, 4.1, 4.2, 4.3
B	Dawnside bow shock and foreshock region	1.2, 1.3, 3.1, 3.2 3.3, 4.1, 4.2, 4.3
C	Dawn flank magnetopause	1.1, 1.2, 2.1
D	Magnetotail	1.1, 1.4, 2.1, 2.2

panel), the spacecraft cross the bow shock, which is primarily quasi-perpendicular in this region and then are mostly in the pristine solar wind, magnetically disconnected from the bow shock. The primary focus for Campaign A is the physics of particle acceleration and dissipation at the quasi-perpendicular shock and turbulence in the undisturbed solar wind.

In Campaign B, the spacecraft are also in the solar wind most of the time. However, they cross the primarily quasi-parallel bow shock and are mostly in the ion and electron foreshock regions magnetically connected to the bow shock. The primary focus of Campaign B is the physics of particle acceleration and dissipation at the quasi-parallel shock and turbulence generated in the foreshock and the downstream magnetosheath.

In Campaign C, the spacecraft skim the magnetopause on the dawn flank tailward of the terminator. The primary focus of this campaign is the stability of reconnection in the presence of fast magnetosheath flow and the importance of secondary reconnection in plasma transfer in KH vortices.

In Campaign D, the spacecraft are in the magnetotail. For the first tail pass of the extended mission, this campaign is conducted similar to the prime mission Phase 2b, the first pass through the tail at 25 R_E apogee in the prime mission. The dayside component of the prime mission had the distinct advantage of two passes through the dayside magnetopause. In the second pass, lessons-learned from the first pass were used to optimize the EDR encounters. Lessons-learned include choices for instrument operation, event selection, and average spacecraft separation. The extended mission provides a similar opportunity to apply lessons-learned from the tail pass in the primary mission to the first tail pass in the extended mission. Fig. 1-1 (bottom panel) shows that the intervals when the spacecraft are within 0.5 R_E of the tail neutral sheet are concentrated on the dusk side. Tail phenomena such as bursty bulk flows are also more prevalent on this side. Thus, there is excellent synergy between the orbit and reconnection phenomena.

In subsequent years, fuel reserves permitting, these campaigns are repeated with one important orbit change and several important changes in the spacecraft configuration. Early in Phase 4a, the orbit apogee is raised to 28 R_E. The increase opens up the possibility to explore the undisturbed solar wind farther from the Earth, investigate particle acceleration deeper into the foreshock, study reconnection on the flanks farther tailward of the terminator, and search for EDRs deeper in the magnetotail. As the fuel level decreases, the tetrahedron formation is allowed to come apart and the spacecraft spread out more and more in a string-of-pearls configuration. This new configuration allows investigation of larger scale phenomena while still maintaining the high cadence measurements that make MMS a unique mission. Table 5.2-1 summarizes the four campaigns and their science focuses. Details of MMS contributions to this new science are discussed in §5.3.

During the extended mission, the focus of MMS research of reconnection will be to:
- Continue research of tail reconnection during a second tail pass, based on lessons learned from the first pass
- Investigate reconnection in environments and configurations undersampled or not available during prime mission
- Verify knowledge from prime mission research regarding universality and applicability to additional regimes and environments

5.3 Prioritized Science Goals

5.3.1 PSG 1: Investigate magnetic reconnection in the near-Earth space environment (G2, G1, G3). The MMS mission has been designed specifically to address the kinetic physics of magnetic reconnection. The unprecedented quality of measurements, combined with state-of-the-art theory and modeling, has led to dramatic new insights, in particular pertaining to asymmetric reconnection at the magnetopause. At the time of this proposal, the first tail phase has not begun, but we expect a similarly large scientific harvest from that phase as well. We also expect that there will be significant lessons-learned from this first tail pass that will be applied in the extended mission. During the extended mission, the focus of MMS research of reconnection will be to:

- Continue research of tail reconnection during a second tail pass, based on lessons learned from the first pass
- Investigate reconnection in environments and configurations undersampled or not available during prime mission
- Verify knowledge from prime mission research regarding universality and applicability to additional regimes and environments

5.3.1.1 Reconnection in the nightside magnetosphere (PSG 1.1). Reconnection in the magnetotail

is the mechanism behind the generation of dynamic phenomena like bursty bulk flows, magnetic field dipolarization, and plasmoid formation and ejection. In contrast to the asymmetric geometry at the magnetopause, tail reconnection features symmetric inflow regions, as well as relatively small values of the guide (cross-tail) magnetic field component. As predicted by theories and models, the cross-tail magnetic field has been observed to be quadrupolar around the reconnection x-point, believed to be around 20-25 R_E during onset and early evolution, and then retreating tailward at velocities of 100s of km/s. Observations further confirm the existence of an ion diffusion region, where ions decouple from the magnetic field, while electrons remain frozen in. GEOTAIL observations indicate that the magnetotail current sheet thins down to ion or smaller scales during reconnection onset, and afterwards in the immediate vicinity of the reconnection region. Plasma temperatures inside the plasma sheet (as contrasted to the lobes; see below) are typically considerably higher than at the magnetopause: ion energies are typically 5-10 keV, and electron energies are around 1 keV. Typical densities are between 0.1-1 cm^{-3}, which has the fortuitous effect that electron scale lengths are between 5 and 15 km and thus readily accessible to tetrahedral sizes obtainable by MMS.

The prime energy source for magnetotail dynamics is the magnetic energy stored and released through reconnection of the lobe field lines. When reconnection occurs in the tail, low-temperature lobe plasma (a mix of solar wind plasma and particles of ionospheric origin) streams along the magnetic field toward the plasma sheet and combines with hotter plasma sheet particles in the kinetic layers surrounding the reconnection diffusion region.

Past spacecraft observations have demonstrated the kinetic nature of magnetotail reconnection on ion scales, but the structure of the electron diffusion region, which is critical to magnetic reconnection, is presently unknown. Plasma parameters in the magnetotail readily permit positioning of multiple spacecraft in the electron diffusion region. Gradients of key plasma parameters can thus be reliably obtained, allowing the validity of proposed reconnection mechanisms in anti-parallel geometries or in geometries with small guide fields to be assessed. Of particular interest is the postulated role of anomalous resistivity in reconnection, which typically involves correlations between parameters such as density and electric field, and the idea that thermal inertia-based dissipation facilitates the electron diffusion region by means of nongyrotropic pressure tensors. Of further interest is the transition from anti-parallel reconnection dynamics to guide-field reconnection dynamics, which is expected to occur for fairly small guide fields because of the easy magnetization of electrons. Asymmetry effects brought about by dipole tilt and similar effects are likely to create situations in which the lobes, and hence the inflow regions, are not completely symmetric. Deviations from symmetry can include different magnetic field gradients (e.g., due to dipole tilt), or asymmetric plasma densities and composition, generated, e.g., by asymmetric ionospheric heating, or asymmetric loading of the plasma mantle. Campaign D will provide a unique opportunity to study magnetic reconnection in the magnetotail for varying degrees of asymmetry.

Initiation of reconnection in the tail, in contrast to the magnetopause, involves overcoming the stabilizing effect of the normal magnetic field component. Under typical circumstances, this magnetic field component magnetizes electrons, which remain glued to the magnetic field and prevent reconnection as well as tearing. Nevertheless, well-known onset mechanisms, such as the formation of thin current sheets, lead to a depression of the normal magnetic field and reconnection onset via electron demagnetization. An alternative point of view, similar to the nonlinear reconnection activity, is that anomalous resistivity provides electron scattering in the thin current layer. MMS will distinguish between these different possibilities.

During the outbound and inbound orbits of Campaign D, MMS will also provide the opportunity to study the kinetic structure of dipolarization fronts (DFs), and after apogee raise, MMS will, at times, encounter plasmoids so that their kinetic structure can be investigated (Fig. 5.3-1). The larger apogee also allows MMS to investigate reconnection lines in retreat, which will permit the study of the underlying causes of this motion.

Finally, the question of how reconnection processes cold inflow plasma to form a hot plasma sheet remains of great interest. While it remains to be seen whether the necessary energization is generated in the immediate vicinity of the reconnection region, it is clear that the nature and composition of the inflowing plasma will have a profound effect on the structure of the diffusion region, at a minimum on ion scales, but possibly even on electron scales.

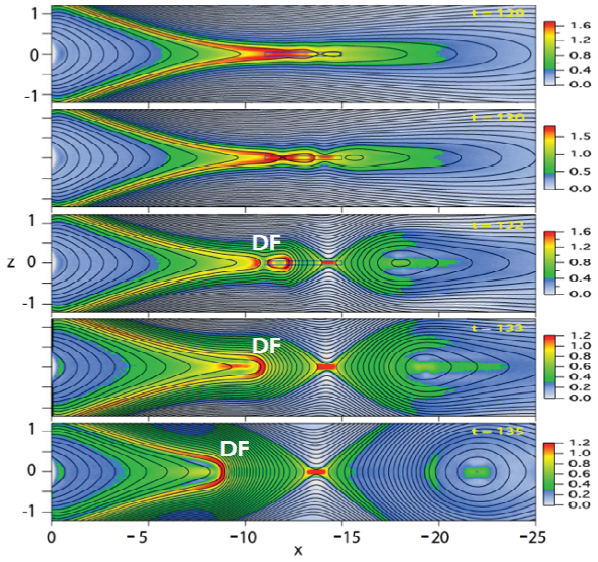

Figure 5.3-1. Simulation of the onset of magnetic reconnection in a tail-like geometry, following solar wind-like driving at the boundary [based on Liu et al., 2014]. The simulation uses realistic ion-electron mass ratios and is used to predict MMS observations during Campaign D.

These effects are largely unknown, with only limited insight based on a small set of numerical model-based investigations. Key questions:

- Which mechanism underlies the electron diffusion region for small or vanishing guide fields?
- How does the electron diffusion region depend on magnetic symmetry?
- How does the electron diffusion region depend on inflow plasma symmetry?
- How does the reconnection rate depend on inflow conditions and symmetry?
- How does reconnection initiate in a current layer with a finite magnetic normal component?
- What is the kinetic structure of BBFs and plasmoids, and why does an x-line retreat?
- How does reconnection process cold inflow plasma, and what is the species dependence?

MMS Approach. MMS will sample the magnetotail current sheet during the extended mission, beginning with the second tail pass (Campaign D). The spacecraft will have sufficient fuel to maintain a tight tetrahedral formation during the extended mission, which will permit the study of kinetic scale gradients. Unlike any mission preceding it, MMS's instrumentation is uniquely designed to address kinetic reconnection physics down to electron scales. Its capability to produce electron distributions every 30 ms has proven extremely successful for studies of magnetopause reconnection, where scale sizes are considerably smaller. Magnetopause reconnection research has shown that MMS measures the reconnection electric and magnetic field, ion composition, ion and electron distributions and their anisotropy, and wave turbulence with unprecedented precision. Low-energy plasma is made measurable by virtue of the ASPOC instrument, which has the demonstrated ability to control the spacecraft potential. With the exception of the larger energy range, for which FPI is designed, however, magnetotail measurement requirements are generally less stringent than those for the magnetopause. MMS is therefore the first and ideal tool to answer these key questions.

5.3.1.2 Magnetic reconnection at the magnetopause, including inside Kelvin-Helmholtz vortices at the tail flanks (PSG 1.2). After the apogee raise in preparation for Phase 2b, the orbit is, by its nature, less well suited to the study of magnetopause reconnection. However, during extended-mission Campaigns A and B, each orbit intersects the nominal magnetopause at least twice, offering further opportunities to study magnetopause reconnection. The data sets obtained during these crossings will be used primarily to verify our understanding obtained during mission Phase 1 or to expand research into new regimes in the case of conditions not encountered previously, e.g., during times of very high solar wind velocity. The nightside magnetopause, on the other hand, has not been explored during the prime mission. There, MMS will encounter very large shear flows between the magnetosphere and the rapidly moving magnetosheath. These shear flows are of great interest – among others because of the reconnection in large shear flow scenarios, and because of the KH instability. Regarding shear flow reconnection, MMS will determine whether there are shear flow conditions under which reconnection is suppressed, such as super-Alfvénic shear velocities. How reconnection is affected by such flow is not well understood. For in-plane flow shear, the well-known Cowley and Owen [1989] prediction is that the reconnection site is stationary if the magnetosheath flow is sub-Alfvénic, convects if the flow is between the magnetosheath Alfvén speed and twice the Alfvén speed, and is suppressed entirely if the flow is faster. However, recently it was suggested [Doss et al., 2015] that (isolated) reconnection sites convect in the presence of any flow and require flows many times the magnetosheath Alfvén

speed to be suppressed. There have been some observational studies on this question [Wilder et al., 2014; Gomez et al., 2016], but much more data is necessary to determine which prediction, if either, is correct.

Strong shear flows also drive the KH instability. Prime mission research has already led to some new insights into KH structure and dynamics. The extended mission, however, will provide much more frequent encounters with KH vortices, and hence enable a dedicated research effort.

Simulations suggest that the KH instability (KHI) develops at the dayside magnetopause when IMF conditions are favorable. Multi-spacecraft (e.g., Cluster) observations demonstrate that the instability grows to a non-linear state on the flanks of the magnetopause (Hasegawa et al., 2004), leading to a large-scale turnover of the KH vortices that mixes the magnetosheath and magnetospheric plasmas (Fig. 5.3-2). Plasma mixing also occurs through reconnection of the undulating magnetopause current sheet [e.g., Eriksson et al., 2016]. MHD simulations, both global and local, show that thin current sheets develop inside the magnetic field, which is twisted by the vortical flow motion. Reconnection can occur in these current sheets, facilitating population mixing and momentum transport from the sheath into the magnetosphere.

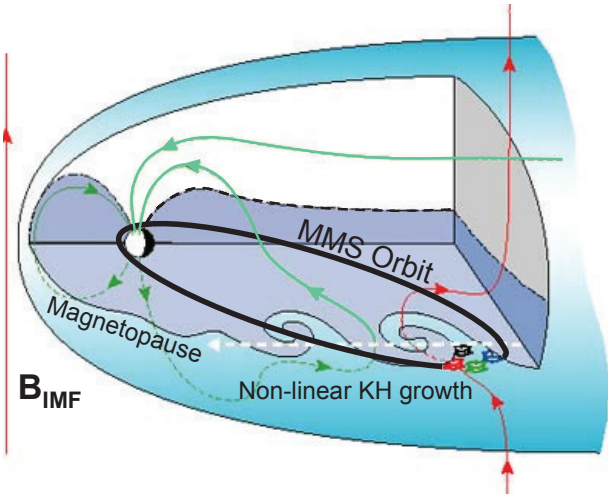

Figure 5.3-2. Three-dimensional cut-away view of the Earth's magnetosphere with the Sun to the left. (Figure adapted from Hasegawa et al., 2004) KH vortices grow to a non-linear state on the flanks of the magnetopause. During the extended mission, the MMS orbit and close spacing of the spacecraft provide a unique opportunity to determine the nature of reconnection in the presence of shear flows and the importance of plasma mixing within the KH vortices.

While the non-linear growth of the KHI on the magnetopause flanks is well-established, its importance for mixing of magnetosheath and magnetospheric plasma is not well understood. In particular, the contribution that reconnection makes to plasma mixing within the wound-up vortices is not yet established [e.g., Nykyri and Otto, 2001; Ma et al., 2014]. Furthermore, the details of this reconnection process (in particular how it might differ from reconnection at the dayside magnetopause) are not well-understood.

MMS Approach. During the prime mission, the MMS orbit apogee was only 12 R_E on the flanks of the magnetosphere. This apogee was optimized for dayside magnetopause crossings, but is too low to regularly observe the non-linear growth of the KHI on the magnetopause flanks. Only one clear KH event was observed in the prime mission [Eriksson et al., 2016], likely due to the arrival of a CME flux rope that provided the conditions for KH growth near the terminator. The MMS orbit apogee is 25 R_E at the beginning of the extended mission and increases to 28 R_E later on. This higher apogee is ideal for investigating the non-linear growth of the KHI, as well as reconnection therein farther down the flanks (see Fig. 5.3-2). The high time resolution and close spacecraft spacing early in the extended mission provide a unique opportunity to investigate ion and electron scale reconnection physics within the wound-up KH vortices that are projected to occur on the magnetopause flanks. Through this multi-spacecraft study, the nature of reconnection in KH vortices and the occurrence and importance of reconnection in plasma mixing in this magnetospheric region will be determined.

5.3.1.3 Reconnection in the solar wind and in the magnetosheath (PSG 1.3). The discovery of reconnection exhausts in the solar wind [Gosling et al., 2005] and in the magnetosheath [Retino et al., 2007; Phan et al., 2007] provided new laboratories where reconnection could be investigated by in-situ measurements. Solar wind and magnetosheath current sheets tend to have stable boundary conditions because they simply convect with the solar wind (and shocked solar wind). Thus these current sheets are ideal for studying the spatial structures of the reconnection layer under well-defined boundary conditions. Furthermore, reconnection could potentially occur in thin current sheets that are generated by

magnetosheath turbulence downstream of quasi-parallel bow shocks [Retino et al., 2007]. It has been suggested that this type of turbulent reconnection could be a means by which turbulence is dissipated and thus it is highly important for space plasmas [Sundqvist et al., 2007].

Plasma measurements on previous spacecraft missions could not resolve thin magnetosheath turbulent current sheets (which typically convect past a spacecraft in a few seconds or less). Thus the occurrence rate of reconnection, and consequently the importance of reconnection for dissipating turbulence, is not known observationally. Furthermore, the kinetic (electron-scale) physics of reconnection could not be addressed in the few magnetosheath reconnection events that have been reported because of the lack of high-resolution plasma measurements on previous spacecraft.

Similarly, in the solar wind, previous spacecraft could only study the large-scale structures of reconnecting current sheets. Thin slow-shock like structures bounding reconnection exhausts where magnetic energy dissipation and plasma heating are theorized to take place could not be resolved by previous plasma measurements.

During the prime mission, MMS did sample the solar wind and the magnetosheath regions. However, because of its low (12 R_E) apogee, MMS did not spend much time in the solar wind: only 2 solar-wind reconnection events were captured in burst mode during prime mission. An example of a solar-wind reconnection exhaust is shown in Fig. 5.3-3. MMS did spend more time in the magnetosheath. However, because this region was not a focus of the MMS prime mission, only a small fraction of turbulent magnetosheath current sheets encountered by MMS were captured in burst mode.

MMS Approach. MMS will spend a considerable amount of time in the solar wind during the extended mission, when the apogee will be 25-28 R_E. There will be at least a few reconnection exhausts per day that will be captured in burst mode. Although FPI was not designed to measure the solar wind, the two solar wind reconnection events captured so far indicate that the ion velocity, the electron density, temperature, and velocity moments and distributions are of sufficient accuracy for reconnection studies (see Fig. 5.3-3). The 30 ms electron measurements reveal the locations of dissipation and heating, as well as the kinetic processes that operate in those regions.

Magnetosheath reconnection will be a high priority during the extended mission as well. This prioritization highlights the flexible nature of the MMS mission operations. Much more burst data will be selected in turbulent current sheets downstream of quasi-parallel shocks to determine the role of reconnection in dissipating turbulence energy.

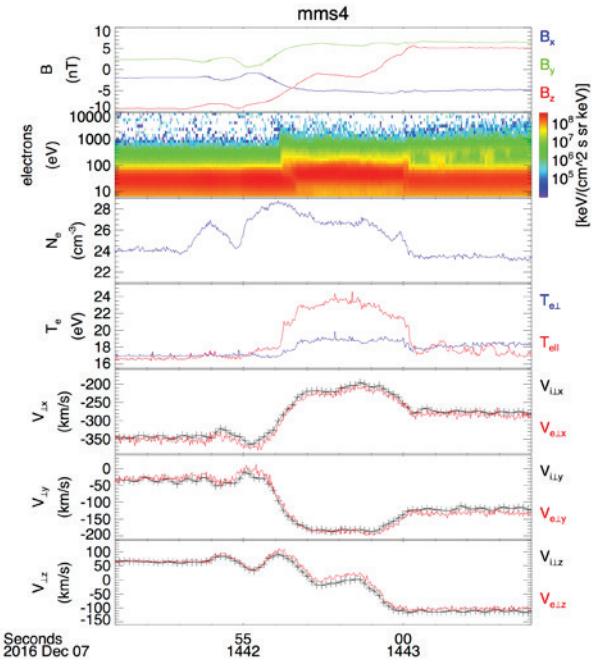

Figure 5.3-3. MMS4 detection of a solar wind reconnection exhaust, demonstrating the high quality of burst-resolution plasma and field measurements in the solar wind. (a) Magnetic field, (b) electron energy flux antiparallel to the magnetic field, (c,d) electron density and temperature, and (e-g) perpendicular ion and electron velocities. The excellent agreement between the ion and electron velocities prove the accuracy of the measurements [Phan, unpublished manuscript].

5.3.1.4 Reconnection spatial scales (PSG 1.4). In its tetrahedron configuration, MMS operates as a precision instrument, which is designed to resolve the small spatial gradients of importance to understanding the kinetic underpinnings of magnetic reconnection. Near the end of the extended mission, fuel depletion may require a string-of-pearls geometry, which is well suited to investigate the macroscopic coherence of kinetic physics, e.g., determine the length of a reconnection line and the processes responsible for it.

Simulations have shown that fast flows from the reconnection site are associated with low-entropy, dipolarized magnetic flux bundles (DFBs or "bub-

bles") [e.g., Birn et al., 2009]. While observations cannot directly provide the entropy content of field lines or flux bundles, proxies have been developed to estimate the field line entropy, which support this view for observed dipolarization events [e.g., Wolf et al., 2006, 2009; Dubyagin et al., 2011]. Simulations have also demonstrated that the cross-tail extent of the fast flows or DFBs may be significantly smaller than the extent of an x-line, which is apparently related to a more significant reconnection rate and entropy reduction limiting the region of fast flows. It is not understood, however, what determines this scale size and why reconnection becomes faster only over a limited cross-tail extent. Simulations indicate a possible relationship to interchange modes, ignited prior or to after reconnection [Birn et al., 2011; Pritchett and Coroniti, 2013].

MMS Approach. Determining the macroscopic dimensions of a reconnection region, as well as causes for them, be they micro- or macroscopic, requires both an accurate determination of the electric field, of the boundaries of the region of fast reconnection and of the local physical conditions that might distinguish that region from the surroundings. In the extended phase MMS will provide local gradients but at some later time, when the tetrahedron configuration dissolves into a "string-of-pearls" configuration with different inter-spacecraft separations, the multi-scale spatial extent will become measurable through simultaneous observations from the more dispersed MMS platforms. MMS will therefore provide the opportunity to associate local, kinetic conditions to macroscopic dimensions associated with the reconnection process.

5.3.2 PSG 2: Study the processes that heat plasma populations and accelerate particles to large energies (G3, G1, G2). Like magnetic reconnection, processes that heat or accelerate particles to high energies find broad application in plasmas outside of the magnetosphere, from astrophysics to solar physics, and in interplanetary space, e.g., in association with propagation of coronal mass ejections. MMS measurements—in particular those in the magnetotail—will reveal whether and how particle acceleration is associated with magnetic reconnection and how reconnection or processes resulting from reconnection can heat plasmas.

5.3.2.1 The dissipation of magnetic energy during reconnection – electron and ion heating (PSG 2.1). Magnetic reconnection leads to the release of magnetic energy. This energy ultimately appears in electron and ion thermal energy and bulk flow. In the context of the essentially collisionless magnetosphere, distribution functions are typically non-Maxwellian so the proper measure of this heating is the second moment of the distribution functions. At the magnetopause (Phan et al., 2013, 2014) and in the magnetotail (Eastwood et al., 2013), the ions typically gain more energy than the electrons during reconnection. While magnetic energy dissipation takes place in the electron and ion diffusion regions, because of its larger volume, much of the energy is released downstream in the reconnection exhaust.

The mechanisms for electron and ion heating and, in particular, the partitioning of energy between the two species (or other ion species) is not well understood. Ion distributions typically take the form of counter-streaming beams (Hoshino et al., 1998) that are produced as a result of reflection off reconnected field lines in the expanding exhaust (with energy gain scaling like $m_i V_A^2$). However, the measured ion thermal energy is much less than expected from the counter-streaming picture (Phan et al., 2014). Electron heating is reduced compared with that of the ions but exhibits similar scaling. It is even less well understood than ion heating. In single x-line reconnection, a single electron encounter with an expanding reconnected magnetic field produces negligible energy gain. Particle-in-cell (PIC) simulations suggest that a field-aligned potential develops that prevents hot electrons in the exhaust from expanding into the upstream region and leaving the ions behind (Egedal et al., 2008, Haggerty et al., 2015). Such a potential enables electrons to have multiple interactions with expanding reconnected field lines and therefore boosts electron energy gain. Electrons can also gain energy through the interaction with growing and merging magnetic islands (Drake et al., 2006, Oka et al., 2010). High-frequency turbulence is often measured in the diffusion region, along magnetic separatrices, and within the exhaust (Eastwood et al., 2009) but the role of this turbulence in the dissipation of magnetic energy and particle heating remains unclear.

MMS Approach. The unique capability of MMS to measure the electron and ion 3D particle distribution functions with very high cadence as the reconnection diffusion regions and exhausts are crossed will facilitate the exploration of all of the mechanisms for electron and ion heating. At the magnetopause in particular data from full crossings of the exhaust and diffusion region will yield both

upstream conditions as well as the particle distributions and energy gain as reconnection proceeds. A key ingredient will be to use the measured distributions to infer the presence and magnitude of the field-aligned potential to determine its role in the heating of both species as suggested by recent simulations and theory. The direct measurement of weak large-scale, parallel electric fields is not feasible but electron distributions can reveal the structure of the potential (Egedal et al., 2008) so that its role can be assessed. The recent MMS observations of the filamentary structure of the reconnection exhaust (Phan et al., 2016) motivates exploration of the role of turbulence in particle heating. During reconnection in the magnetotail, MMS high cadence measurements will enable the exploration of the relative roles of the exhaust and the dipolarization front in heating electrons and ions.

5.3.2.2 Particle acceleration by dipolarization fronts (PSG 2.2). Charged particle acceleration can occur at the reconnection site itself. Simulations indicate the possibility that more efficient acceleration may be related to the impulsive electric field associated with flow bursts from the reconnection site associated with magnetic field dipolarization fronts (DFs) [Nakamura et al., 2002; Runov et al., 2012]. Test particle tracing in the electromagnetic fields of MHD simulations of reconnection and dipolarization [e.g., Birn et al., 2015] have indicated two sources and entry mechanisms into the acceleration region: cross-tail drift from the near-tail plasma sheet flank regions and entry by reconnection of field lines extending into the more distant tail.

During the commissioning phase MMS provided detailed ion velocity distributions in the magnetotail. Observations near the plasma sheet boundary layer (PSBL), reveal multiple beams parallel and antiparallel to the magnetic field (Fig 5.3-4). Particle tracings in the MHD fields of a simulation of reconnection and dipolarization have produced rather similar ion distributions in the vicinity of the PSBL (Fig. 5.3-5). These simulations have begun to shed light on the acceleration mechanisms: the lowest energy beams are accelerated at an earthward propagating DF, while higher-energy beams have experienced multiple acceleration, first at the reconnection site, then at the DF, with mirroring in Earth's dipole field in-between.

Beyond proving the basic mechanism, important questions remain: What determines the cross-tail extent of the flow bursts and energetic particle injections? What affects anisotropies of ions and electrons? What is the cause of the occasional events that show injections of one or several MeV particles? What is the effect of kinetic scale features associated with DFs?

MMS Approach. The above questions will be answered by the combination of simulations with detailed high-resolution particle observations, not only earthward but also tailward of the reconnection site. During most if not all of the extended mission, MMS will maintain a tight tetrahedron that naturally focuses on the local aspects of these acceleration processes. We will determine if magnetic island compression can lead to substantial electron acceleration and investigate the local physics involved in

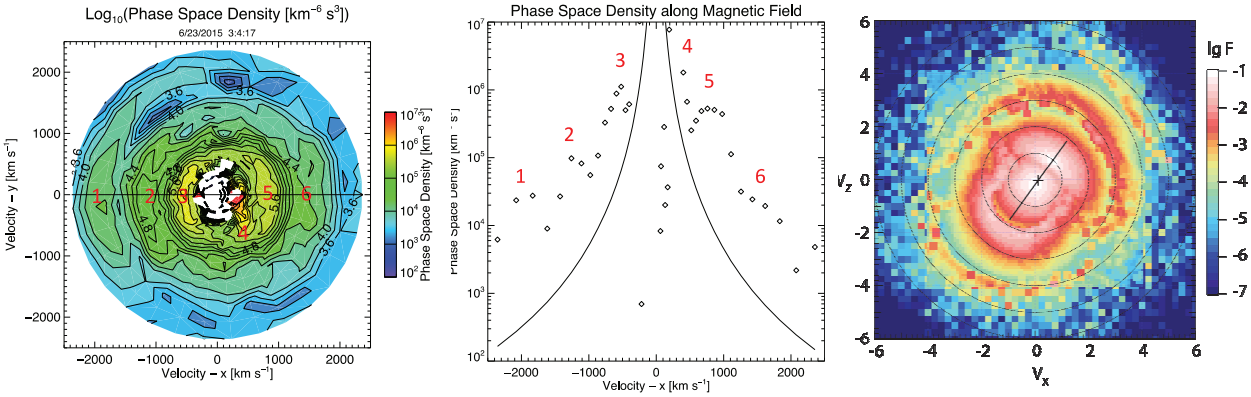

Figure 5.3-4. Left and center: Ion velocity distribution observed by MMS in the vicinity of the plasma sheet boundary layer during the commissioning phase. The distribution shows evidence of multiple beams at increasing energy levels. Right: The same, obtained by tracing particles in MHD simulations. The cross indicates the bulk flow velocity and the black line the magnetic field direction. Dedicated particle energization studies during the extended mission will determine the origin of these beams. (Birn et al., in preparation, 2017)

accelerating particles in depolarization fronts. The string-of-pearls configuration much later in the extended mission naturally lends itself to the exploration of larger-scale spatial dimensions and of the processes setting those scales.

5.3.3 PSG 3 Study the way turbulent processes interact on kinetic scales (G1, G2)

5.3.3.1 Turbulence in the Magnetosheath and Solar Wind (PSG 3.1). Plasmas in the heliosphere are typically turbulent, often exhibiting large amplitude fluctuations in the fields and plasma moments. The plasmas sampled by MMS are no exception — both the solar wind and magnetosheath show significant spatial and temporal fluctuations. A basic property of turbulence is that turbulent energy cascades or transfers from long length- and time-scales to small length- and time-scales. Ultimately, at very small scales, turbulent energy is dissipated and plasma internal energy increases (heating). Such dissipation plays an important dynamical role in many heliospheric plasmas, representing a fundamental plasma physics problem with applications to diverse systems such as the solar corona, the solar wind, the magnetosheath, accretion disks around protostars and black holes, and laboratory plasmas including fusion devices. Numerous specific mechanisms to facilitate this dissipation of turbulent energy have been proposed, such as collisional resistivity and viscosity, Landau damping, stochastic heating, and magnetic reconnection and processes associated with current sheets and other coherent structures.

In low-collisionality space plasmas, the turbulent energy must be dissipated by kinetic mechanisms often at length and time scales where viscous and resistive closures are not applicable. Furthermore, kinetic processes involve non-local effects where the plasma is not in thermodynamic equilibrium. Because of this complexity, the pathways and mechanisms leading to plasma dissipation are neither unambiguously identified nor well understood. More specifically, the properties of turbulence at smaller non-MHD scales have not been adequately characterized from observations. At the relevant small length scales and high frequencies, single spacecraft observations suffer from uncertainty in whether the fluctuations measured are spatial or temporal in nature. While coherent structures (e.g., current sheets) have been studied at larger scales in both the solar wind and magnetosheath, whether they are dynamically important for kinetic dissipation remains to be determined. In the prime mission, MMS has had limited opportunity to study turbulence in the solar wind and magnetosheath because its apogee was only 12 R_E. However, the limited measurements in the pristine solar wind near the Earth's bow shock (see Fig. 5.3-5) demonstrate the potential for unique contributions from MMS on turbulence in the solar wind. The preliminary studies in the magnetosheath [e.g., Yordanova et al., 2016] demonstrate the need to select specific magnetosheath events (e.g., velocity shears and reconnection events) to understand the role of turbulence in heating and acceleration.

MMS Approach. During Campaigns A and B, the higher orbit apogee of MMS presents an unprece-

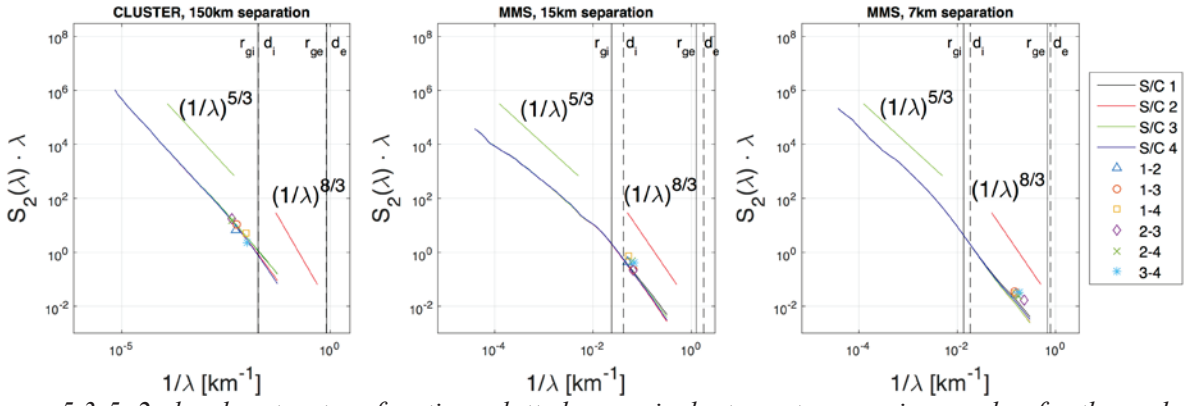

Figure 5.3-5. 2nd order structure function, plotted as equivalent spectrum vs. inverse lag for three observations in the solar wind. Left to right: 30 minutes of Cluster data (February 2002, spacecraft separation ~150 km); 5 minutes of MMS data (November 2015, separation ~15 km); 6 minutes of MMS data (December 2016, separation ~7 km). Ion and electron scales indicated as vertical lines for gyroradii (solid) and inertial scale (dashed). The MMS data suggest a change of the turbulent cascade below ion scales. The capabilities of the MMS mission and the higher apogee in the extended mission allow the study of turbulence below the ion scales well into the kinetic range.

dented opportunity to study solar-wind turbulence at scales extending well into the kinetic regime. These timely studies complement and extend substantial current interest based on theory and simulation; however, MMS instrumentation enables the first direct observations of this important regime, which is of fundamental importance in understanding dissipation, heating, and energy flow in space plasmas.

Solar Wind: MMS will make important new contributions to studies in solar-wind turbulence. FPI electron measurements capture the fundamental flow parameters (density, vector velocity) at unprecedented resolution and cadence. With over an order of magnitude increase in ion measurement cadence, the rapid evolution of crucial kinetic features and sub-populations of non-thermal and accelerated ions upstream and within the shock transition will be accessible for the first time. Complemented by high time cadence and direct fine spatial resolution measurements at four spacecraft positions, MMS will reveal fine-scale magnetic and electron structure and dynamics in turbulence, current sheets, shock layers and other regions. Providing a unique high cadence, fine-spatial-scale capability, MMS will reveal details of microphysical processes and an unraveling of space-time structure at a level never before possible. An example solar wind event is shown in Fig. 5.3-6, which shows that even though FPI is not designed to measure solar-wind cold ion beams, it is uniquely suited for measuring the fluctuations that result from turbulence.

Magnetosheath: MMS will make unprecedented measurements of turbulent structure in the magnetosheath at kinetic scales. Initial studies with MMS data from the prime mission have probed electron scales (Yordanova et al., 2016), ion scales (Huang et al., 2016), and k-space structure (Narita et al., 2016). MMS high-resolution particle measurements, magnetic field, 3D electric field and high energy particle data, combined with the small separation of the spacecraft, will for the first time be able to measure kinetic processes at the scales where turbulent energy is dissipated. For example, direct measurements of wave-particle interactions at electron kinetic scales are possible. In addition, Campaigns A and B (see §5.2.2) enable selection of events where coherent structures will be fully resolved, allowing direct measurements of the possible role of, e.g., magnetic reconnection in the magnetosheath and in velocity shears. Coupled with theory and simulations of turbulence, it will be possible to probe distribution functions to directly determine the kinetic mechanism dissipating the turbulent energy. These contributions will lead to a far more complete picture regarding particle heating and acceleration and turbulent dissipation at kinetic scales.

5.3.3.2 Pickup ions (PSG 3.2). Interstellar neutrals freely enter the solar system and have been observed at 1 AU by IBEX. These neutrals undergo charge exchange in the inner solar system and are

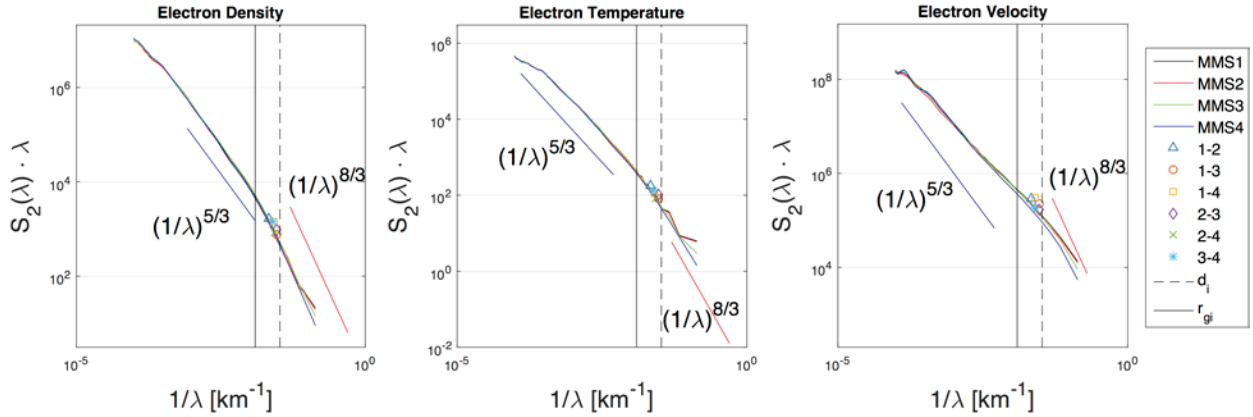

Figure 5.3-6. 2nd order structure functions of electron (a) density, (b) temperature and (c) velocity from three minutes of burst FPI data (v3.1.0) in Earth's magnetosheath, all plotted as equivalent spectra vs inverse scale. Shown are estimations from single spacecraft (solid lines) at spacecraft separation scale, and two-spacecraft (symbols). Ion scales indicated are gyroradius (solid vertical line) and inertial length (dashed). Reference lines indicate slopes of -5/3 and -8/3. The 30 ms resolution and 10s of km spacecraft separation are orders of magnitude better than previous satellite observations. The focused study of magnetosheath turbulence in the extended mission will determine the kinetic mechanisms for turbulent energy dissipation.

picked up by the solar wind. There have been observations of the pickup ion distribution functions from STEREO and composition measurements from ACE and SOHO. The pickup ions mass load the solar wind and, through wave-particle interactions and solar wind turbulence, these ions scatter into a shell distribution that, at the termination shock at 100 AU, exceed the pressure and temperature of the bulk solar wind ions.

Pickup ions are mostly singly charged because the probability of a second charge exchange following the first exchange is very low. Nonetheless, multiply charged pickup ions have been observed in fairly high concentrations. It has been postulated that interstellar neutrals passing through dust in the inner solar system create multiple charge states similar to the passage of neutrals through a thin carbon foil [e.g., Collier et al., 2003]. This same process may produce multiply charged pickup ions (He^{2+}, O^{2+}) and limited measurements in the solar wind by MMS in the prime mission show these pickup ions. However, because the 3-D measurements of the distributions are rare, the nature of this dust and the implications for scattering in the turbulent solar wind are not known.

MMS Approach. The Hot Plasma Composition Analyzer on MMS uses a unique system to suppress high H^+ fluxes without affecting heavier ion fluxes. When the spacecraft are in the solar wind, this instrument measures full 3-D, mass-resolved pickup ion distributions. In the extended mission, the spacecraft spend days in the solar wind over a period of approximately 8 months approximately centered on the interstellar neutral downwind direction (i.e., in the focusing cone). In Campaigns A and B, specific intervals of pristine solar wind (without contamination from energetic ions from the bow shock and magnetosphere) will be selected. The 3-D distributions measured during these intervals help determine the scattering mean free path for forming pickup ion shells in the outer heliosphere. Understanding the concentrations of singly and multiply charged ions, their distribution functions, and their distribution in the downstream focusing cone promises to reveal the nature of the inner solar system dust and the degree of scattering for pickup ions, which is critical for understanding ion dissipation in the outer heliosphere and at the termination shock.

5.3.4 PSG 4: Investigate the microphysics of collisionless shocks (G2, G1, G3)

5.3.4.1 Transient ion foreshock phenomena (PSG 4.1). Ion foreshocks [e.g., Eastwood et al., 2005] form in the quasi-parallel region upstream of supercritical shocks in collisionless plasmas owing to particle acceleration at the shock and reflection back into the incident upstream plasma. Ion kinetic effects in this region lead to the development of large-scale (several to >10 R_E) transient ion foreshock phenomena (TIFP), such as hot flow anomalies, foreshock cavities, short large-amplitude magnetic structures, and foreshock bubbles [e.g., Sibeck et al., 2002; Turner et al., 2013; Wilson et al., 2013]. These transient structures form multiple times per day upstream of the terrestrial bow shock [e.g., Turner et al., 2013] and may play an important role in impacts on the magnetosphere-ionosphere system [e.g., Plaschke et al., 2013; Archer et al., 2015] and in particle acceleration [e.g., Wilson et al., 2016]. Before MMS, the only multipoint observations allowing for the study of the formation and spatiotemporal evolution of TIFP were from the THEMIS and Cluster missions. These observations were done at large spacecraft separations with time resolutions of the order of seconds. During the prime mission MMS made initial observations of TIFPs (Fig. 5.3-7), indicating the potential for further research.

The processes in these foreshock structures at electron scales are not well known; in particular, the nature of electron-scale energy dissipation in the foreshock region, and whether it presents any significant contribution on global scales is not understood. Furthermore, the fine-scale internal structure (total pressure balance, current systems, wave environment, etc.) of different TIFPs and how this structure compares to our current best estimates from state-of-the-art models is in need of exploration, as is the role of electron scale processes in the formation and evolution of different types of TIFP. Finally, we need to understand the acceleration mechanism responsible for generating >100 keV electrons within various TIFP [e.g., Wilson et al., 2016] and determine whether shock-shock interactions between TIFP and the bow shock result in significant particle acceleration upstream of the bow shock. These questions have important implications for the impact of TIFP on Earth's magnetosphere-

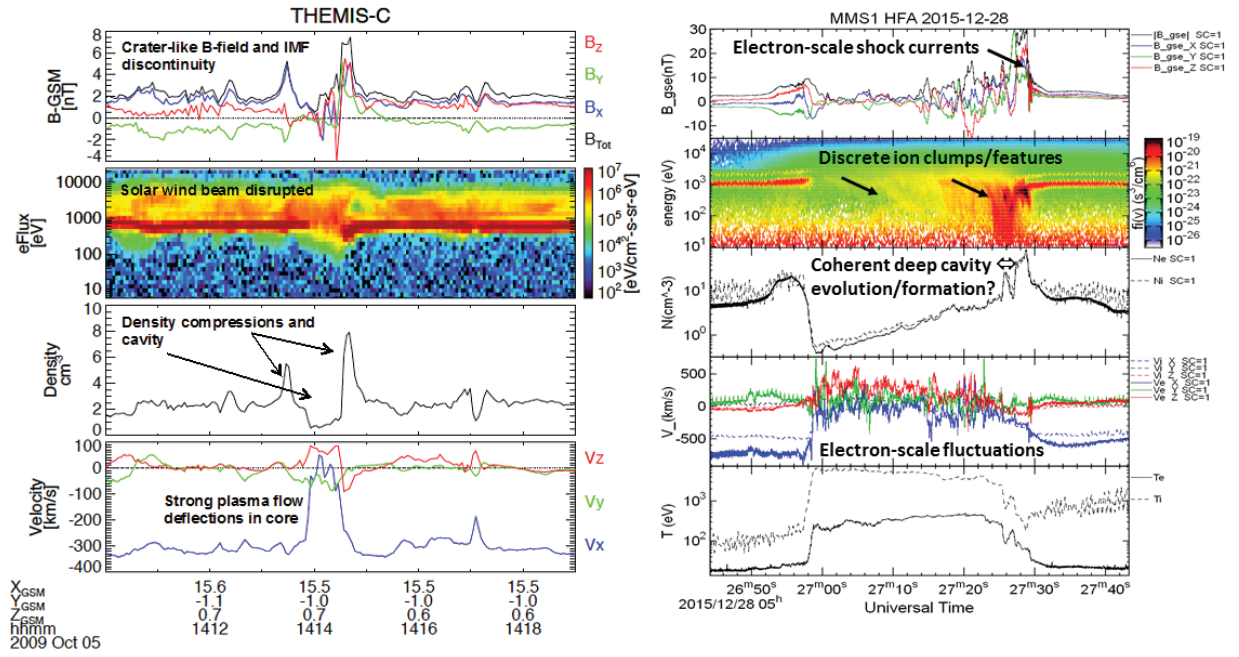

Figure 5.3-7. Example of hot flow anomalies observed by previous missions (left) and MMS (right). Note the change of scale from ~9 minutes to 1 minute. The annotations illustrate the main ion features already known and the areas where MMS will investigate issues of formation and electron-scale physics in the extended mission. Panels show magnetic field, ion spectra/phase space density, density, bulk velocity and temperatures. This example shows the power and promise of MMS to resolve electron scales in the foreshock (unpublished THEMIS and MMS data courtesy of D. L. Turner and S. J. Schwartz).

ionosphere system, developing our interpretation and theory of TIFP at other planets and astrophysical systems, and re-evaluating concepts and theory of particle acceleration in astrophysical plasmas throughout the universe.

MMS Approach. In Campaigns A and B, MMS spends much of its orbit upstream of the bow shock, including long periods in the quasi-parallel foreshock. MMS provides a unique set of high-resolution particle, field, and wave data, which allows significant progress toward answering many of the above-listed science questions. This targeted burst-mode campaign delivers the opportunity for studies of different types of TIFP on both an in-depth case study basis, revealing dissipation and acceleration processes, and at a statistical level contrasting the dynamics over a range of conditions. MMS's advanced instrumentation along with the 4-point tetrahedron multipoint nature of the MMS constellation thus provides routine opportunities to study foreshock processes and the formation and evolution of various TIFP at currently unexplored electron scales.

5.3.4.2 Electron heating in collisionless shocks (PSG 4.2). In the collisionless interplanetary medium, shock waves are responsible for both heating and selective acceleration of different sub-populations of particles. The fraction of the shock energy budget that goes into bulk electron heating, which also is believed to support self-consistently the macroscopic DC cross-shock electric potential, decreases with increasing shock Mach number [Ghavamanian, 2013]. Collisionless shock environs are also rich in electromagnetic fluctuations [Wilson et al., 2014]. Recent MMS results [Goodrich et al., in preparation, 2017] confirm that many of these fluctuations in the shock ramp are not wave-like oscillations or simple features [Walker et al., 2004] but instead are short-scale coherent structures involving large (200 mV/m) parallel electric fields, including double layers or phase space holes (Fig. 5.3-8), and suggest that a dense patchwork of such structures could unify the DC and AC perspectives.

There is no quantitative prediction for how much energy ends up in different forms, e.g., electron heating, proton and alpha particle heating and energetic ion acceleration, as a function of the upstream conditions. The answer is in the detail of what happens within the relatively sharp shock transition itself, or even within the thin current layers associated with

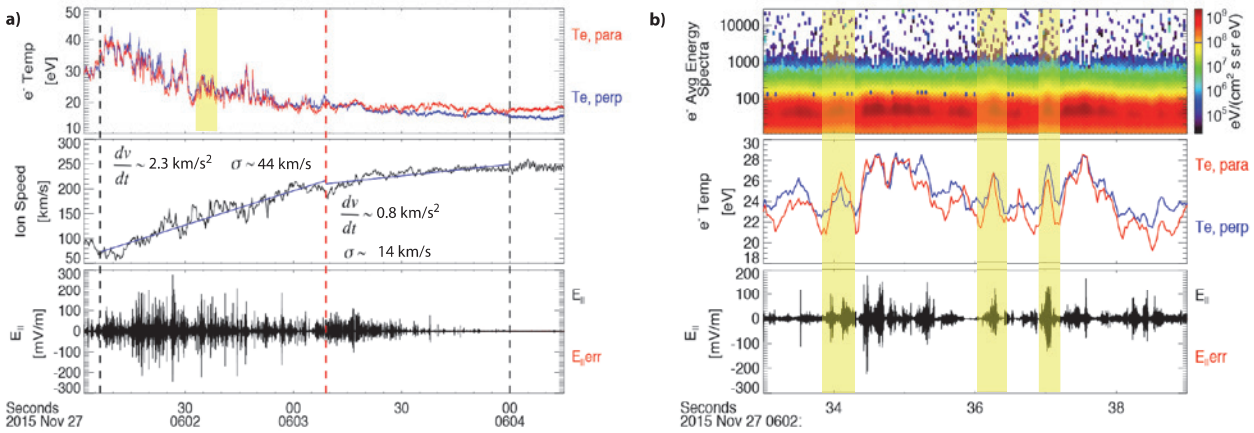

Figure 5.3-8. This figure shows observations during an oblique bow shock crossing (42 degrees). The temperature enhancements in the six-second close up (panel b) occurred in the magnetically turbulent area within the "foot" of the shock. This electron heating in thin current layers will also be investigated in interplanetary shocks in the extended mission (Goodrich et al., in preparation, 2017).

waves present around this main transition, not just characterization of the upstream and downstream states. While previous missions, notably Cluster, have explored the ion-scale physics, they are unable to resolve the collective processes that thrive in the sharp shock transition on electron scales.

MMS Approach. During the primary mission, MMS encountered and returned the highest resolution data for nearly 300 terrestrial bow shock crossings. These data sets form the basis for initial investigations and proof of concept that will be implemented in the extended mission. Given the relatively low apogee, MMS only exited the Earth's magnetosheath under extreme solar wind conditions (e.g., ICME or fast solar wind periods). Interplanetary shocks are absent from the dataset because it usually took the strong interplanetary shock from an ICME to force MMS into the solar wind. Quantifying the contributions of double layers, phase space holes, waves, and energy channels requires (a) a statistical sample covering large swathes of shock Mach number, geometry, and plasma conditions and (b) resolution in both space and time of the electron-scale dynamics (tens of km and tens of milliseconds). The MMS plasma instrumentation has the necessary time resolution to investigate electron-scale dynamics and put these dynamics in the context of the ion scales. The quality of the MMS 3D electric field data afforded by the combined spin-plane wire booms and axial booms enables the role of parallel fields to be firmly established for the first time. This instrumentation, coupled with the higher apogee to observe shock crossings at a wider range of conditions and the maintenance of the close spacecraft configuration guarantee important progress in understanding the energy partition in collisionless shocks. Of particular importance is extending the preliminary work at the Earth's bow shock to interplanetary shocks. The understanding of electron scale physics at these shocks paves the way to understanding how interplanetary shocks modify the solar wind and pick up ion populations as the shocks propagate away from the Sun.

5.4 MMS in the Heliospheric System Observatory

With comprehensive multi-instrument measurements, the four MMS spacecraft play an integral role in the Heliospheric System Observatory. Throughout the extended mission, there are numerous occasions when the MMS spacecraft are serendipitously located to play either an adjunct role or a central role in correlative studies with other missions. The planned orbits of the MMS spacecraft will provide ample opportunities for multi-mission studies of the near-Earth space environment. Possible scientific foci are too numerous to discuss here; instead, the five examples discussed below are associated with the extended mission PSGs discussed above. These serve as representative examples, and the contributions from the MMS instrument suites to these studies are shown in Table 5.4-1.

5.4.1 Particle energization at the bow shock and foreshock (PSG 2, 4). Understanding the nature of particle energization is a key heliophysics objective. In the extended mission, MMS is frequently located

Table 5.4-1 MMS instrument contributions to the Heliospheric System Observatory Studies				
Heliospheric System Observatory Correlative Study	FPI	HPCA	FIELDS	EPD
5.4.1 Particle energization at the bow shock and foreshock	S	P	S	P
5.4.2 Effects of upstream structures on the magnetosphere	P	S	P	S
5.4.3 Nature and Extent of reconnection in the magnetotail	P	S	P	S
5.4.4 Transport & energization of plasma from the tail into the near-Earth magnetosphere	P	P	P	P
5.4.5 Shock and reconnection line dimensions in the solar wind.	P	S	P	S
P = primary contributions to the science, S = secondary or supporting contributions to the science				

within the foreshock, a region where several distinctly different energetic ion and electron populations are observed. The origin of these populations has been controversial from their first observations more than 4 decades ago. They are likely from multiple sources, Fermi acceleration of solar wind ions in the turbulent foreshock and quasi-parallel shock region re-acceleration of suprathermal solar and interplanetary particles at various portions of the bow shock, and "leakage" of the energetic population in the Earth's magnetosphere along field lines that thread the foreshock.

With an apogee of 25 R_E during its extended mission, MMS will spend prolonged periods of time within the foreshock, where it will measure ion composition and electrons with energies up to >1 MeV. Composition is one key to distinguishing the two potential sources. As Fig. 5.4-1 top panel illustrates, Geotail and Cluster will often lie upstream from the bow shock or within the magnetosheath when MMS observes foreshock ion and electron events. The combined observations determine plasma characteristics as a function of distance from the bow shock, local time, and connection to the magnetosphere. ACE and Wind observations are used to identify potential seed populations within the solar wind. This multi-mission study resolves when and where diffusive acceleration and leakage from the ionosphere dominate and defines the effectiveness of diffusive acceleration at shocks.

5.4.2 Effects of upstream structures on the magnetosphere (PSG 4). Processes operating upstream of the shock within the foreshock modify the solar wind just prior to its interaction with the bow shock and have a significant impact upon the magnetosphere. To date a host of transient phenomena have been identified within the foreshock, including hot flow anomalies, bubbles, and cavities. Even today the amplitudes of these transients and, more importantly, how they evolve across the bow shock and into the magnetosphere are still not known. The spacecraft configurations in Fig. 5.4-1 (top) persist as the orbits precess to the dawnside. When one of the spacecraft lies downstream from the shock, these observations can be used to determine whether the pressure variations associated with the foreshock structures are transmitted to the magnetopause e.g., in the form of flow jets and the amplitude of the perturbation of the magnetopause boundary driven by the transients. When prolonged (multi-hour) foreshock perturbations are observed, Van Allen Probes, ERG, and GOES observations may show evidence of enhanced outward radial diffusion that results in, e.g., the rapid loss of energetic electrons from the Earth's radiation belts. Completion of the study provides comprehensive surveys of the various structures generated within the foreshock, their amplitudes and occurrence patterns, their evolution with time, and their impact upon the magnetosphere.

5.4.3 Nature and extent of reconnection in the Earth's magnetotail (PSG 1). The microphysics of tail reconnection is a key objective of the primary mission of MMS. However, reconnection x-lines in the tail extend over macroscopic distances, with an average cross-tail length of 6 R_E during moderate substorms [Nagai et al., 2015, and references therein], and their spreading has been the subject of numerous simulation studies [e.g., Shepherd and Cassak 2012, and references therein]. The ultimate extent of the reconnection line probably depends on IMF orientation, but whether it forms instantaneously over a wide region or spreads with time is not known.

The MMS spacecraft spend extended periods within the magnetotail. Fig. 5.4-1 (bottom) shows that simultaneous MMS, Cluster, and Geotail observations in the tail provide the opportunity to determine the instantaneous extent and spreading of the reconnection line through multi-point measurements extending many R_E. Therefore these measurements distinguish among the possible models for the tail reconnection line extent even before the MMS con-

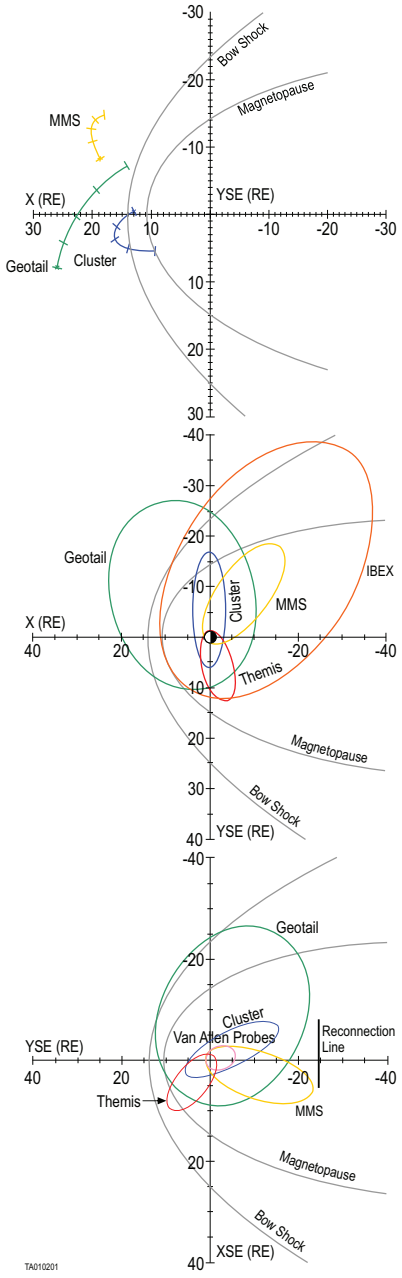

Figure 5.4-1. Orbits of missions in the Heliophysics Systems Observatory in three configurations during the MMS extended mission. (top) Spacecraft in a configuration in the upstream region for studying foreshock phenomena and their effect on the bow shock and magnetopause. (middle) Missions in a configuration for studying the downstream propagation of transients. (bottom) Missions in a configuration for studying the formation of the near-Earth neutral line and transport and energization of plasma throughout the magnetosphere. These sample configurations demonstrate the breadth of the correlative studies in the extended mission.

stellation enters its string-of-pearls configuration.

5.4.4 Transport and energization of plasma from the tail into the near-Earth magnetosphere (PSG 1 & 2). The transport of plasma from the tail and its energization and loss in the near-Earth magnetosphere is a global magnetospheric process that requires the full mission complement of the HSO. Central to the transport of plasma within the magnetosphere is the near-Earth reconnection line. As Fig. 5.4-1 (bottom) shows, MMS is near this reconnection line and determines when the line forms and measures the energy and composition of the plasma injected into the magnetosphere. THEMIS lies in the dayside magnetosphere where it observes the westward drifting clouds of ions injected by the nightside substorm activity. The Van Allen Probes lie deep within the nightside magnetosphere, where they determine the depth particle injections penetrate into the inner magnetosphere and how this depth depends on plasma characteristics of the injections. Other assets (not shown) include TWINS, providing global imaging of the injected ring current plasma, IBEX, providing images of the magnetotail from the dusk flank and observes the tail disconnection created by near-Earth reconnection; and ARTEMIS, in orbit around the Moon observing the expulsion of plasma down the tail. The full Heliophysics Systems Observatory provides unprecedented coverage, both in terms of area and in terms of flux, composition, and energy, of this global transport process that initiates in the vicinity of the MMS spacecraft.

5.4.5 Shock and reconnection line dimensions in the solar wind (PSG 1, 4). There are now three in-situ fields and particles spacecraft near the Sun-Earth first Lagrange point, around 250 R_E upstream of Earth. ACE, Wind, and DSCOVR all provide solar wind thermal particle and interplanetary magnetic field observations. Their large Lissajous orbits around the L1 point often separate these spacecraft out by more than 100 R_E in a plane mostly perpendicular to the Sun-Earth line. MMS solar wind observations provide the crucial fourth set of observations at the tip of a huge tetrahedron to separate spatial and time gradients on this larger scale. In particular, the curvature of interplanetary shock and discontinuity surfaces on the scale-length of the magnetospheric size will be established for the first time. In addition the extent of reconnection lines in the solar wind will be determined, with MMS also probing the microphysics of these large structures.

Technical Implementation and Budget

6.0 Technical Section

6.1 Instrument Status

6.1.1 Instrument Performance. The nearly 100 components of the MMS instrumentation continue to operate at full L1 performance level (Table 6.1-1). The instruments remain capable to delivering this performance throughout the remaining prime phases (2a-2b) and the proposed extended mission. Some minor complications are discussed below. The four MMS spacecraft bus subsystems are performing reliably and within design requirements. There are no open subsystem or hardware risks and all hardware is expected to exceed its design lifetime, providing continued reliability for the MMS extended mission.

6.1.2 Instrument Operational Status. All instruments are operating nominally except one component of FIELDS (Table 6.1-2). Details of the operations for each instrument are as follows:

FPI: The DIS and DES have been reconfigured to measure 2 eV - 30 keV ions and 6 eV - 30 keV electrons, respectively, in response to requests by the science community based on analysis of Phase 1a data; both DIS and DES are delivering >95% lossless data through its compression chip. The instruments have been operated per their pre-launch flight plan and weekly monitoring has found no indications of issues with the HV801 optocouplers. The pre-flight mitigation of maintaining a near constant temperature for the FPI detectors appears to have been successful in maintaining the health of those components and it is anticipated that operations will be conducted continuously from Phase 2b onward through extended mission.

FIELDS: On 12 June 2016, there was a micro-meteoroid impact on the long cable of probe 4 (SDP4) of MMS4, as indicated by accelerometers and a slight spin-rate change. This impact severed a single wire, for probe biasing, to that probe, and this probe is no longer accurate enough in the frequency range, DC- ~ 600 Hz. For this range, the FIELDS team has successfully implemented a processing routine that uses the remaining three probes to determine the components in the spin plane. Fig. 6.1-1 shows that the resulting accuracy, using comparison data from all four probes before 12 June 2016, has changed less that the 0.5 mV/m requirement and that there is only a modest increase in noise floor.

Several HV optocouplers in the Electron Drift Instrument (EDI) deflection system were known before launch to exhibit a higher than desirable degradation with time. As the optocouplers reach their maximum drive limit due to this degradation, the modulated electron bean cannot be deflected to parts of the full-sky when the magnetic field is rapidly varying, resulting in loss of successful beam returns for some part of the spin phase. The impact will be the frequency with which EDI measurements of B and E can be compared to those of the magnetometers and double-probes. The EDI team has begun time-management of estimated remaining hours for each spacecraft, which varies from ~600 hours to over 25,000 hours. Given that these calibrations are now understood and stable, and they can still be made over some spin phase after this full-functional lifetime, this degradation should not affect the calibration through extended mission.

In November 2016, the emitting gun with Gun-Detector Unit 2 (GDU2) of MMS2 failed due to an optocoupler fault within the cathode. That unit can now be operated only in ambient mode (detecting rapidly varying electrons). The team is preparing the single GDU electric field mode software, proven on Cluster, that will return electric field mode EDI data to MMS2. Given magnetic and electric calibrations on the other spacecraft and continued nominal operations of the magnetometers and double-probes, the FIELDS L1 objectives are still being met and will return

Table 6.1-1 Instrument Level 1 Performance

L1 Req	Measurement	Cadence	Range	Resolution	Angular	Met?
M10, M30	FIELDS **B** field	10 ms	DC – 6 khz	0.1 nT	Full 3D	✓
M20, M30	FIELDS **E** field	1 ms	DC – 100 kHz	0.5 mV/m	Full 3D	✓
M40	FPI Electrons	30 ms	10 eV- 30 keV	20%	12˚	✓
M50	FPI Ions	150 ms	10 eV – 30 keV	20%	12˚	✓
M60	HPCA Ion composition	10 sec	10 eV – 30 keV	20%	12˚	✓
M70	EPD Energetic electrons & ions	10 sec	To 500 keV	N/A	12˚	✓
M80	Energetic ion composition	30 sec	To 500 keV	N/A	12˚	✓
I70	Potential Control	20 sec	< 4 V	< 0.1 V	N/A	✓

Table 6.1-2 Instrument Operational Status	
Instrument	**Operation Status**
FPI/DES /DIS	Nominal
HPCA	Nominal
FIELDS	Nominal, except SPD4 on MMS4
EPD	Nominal
ASPOC	Nominal

to full status when that software is implemented during Phase 2a. The high time-resolution ambient electron data, which nominally is taken 50% of the time in the region of interest, are not affected by either of these issues and EDI continues to perform nominally.

HPCA: At the start of Phase 1b, the RF energy range (used to reduce the high proton fluxes without affecting the heavier ion fluxes) was expanded from the original 0.5 to ~4 keV to 0.2 to ~4 keV to reduce the high fluxes of magnetosheath protons in the energy range from 0.2 to 0.5 keV. The RF proton flux reduction for MMS1 and 2 is approximately 50% over the energy range and the reduction for MMS 3 and 4 is approximately 90%. The spacecraft are operated differently to bracket the range of proton fluxes in the magnetosphere, boundary layers, and magnetosheath. In the magnetotail, the RF is turned off because the proton fluxes are low enough that flux reduction is not necessary. Gain tests conducted approximately every 6 months indicate that the detector microchannel plates (MCPs) have not aged and it has not been necessary to increase the MCP voltage to increase the gain.

EPD: One of the Energetic Ion Spectrometer (EIS) units (EIS1) turned off its own high voltage after sensing a micro-discharge in its high voltage circuitry. The unit was turned back on to confirm that it is still operating nominally. For Phase 2a the EIS1 high voltage will be restored with procedures in place to automatically repower the high voltage during the next orbit, should the high voltage trip off again. There has been some light contamination in some of the Flys Eye Energetic Particle Spectrometer (FEEPS) detectors, due to penetration of the aluminum entrance foils that are used to prevent protons from striking the electron detectors. While the rapid burst data can easily be filtered on the ground, the project has uploaded masking tables to provide more comprehensive survey data from all spacecraft; thus, the impact is quite manageable.

ASPOC: The Active Spacecraft Potential (ASPOC) emitters have consumed far less indium to date than expected (~1%), due to the lower level of ion currents (10μA per unit), which enable high value of beam efficiency (larger than 96%), and shorter operation times compared to the original planning. Despite this low consumption, ASPOC continues to meet the Level 1 requirement to reduce the overall spacecraft potential to no more than +40 V. Hence, with the same level of operation (50% of the time in the science region of interest), can be maintained throughout the extended mission.

6.1.3 Calibration Status. The MMS instrument suite continues a vigorous calibration program to ensure L2 data is available in the SDC 30 days after receipt of data. Calibrations and corrections are continuously updated within each instrument complement and across instruments: they are mature and the data products exceed Level 1 requirements. Cross-calibrations utilize independently computed parameters such as currents or densities (e.g., using FIELDS values of upper hybrid frequency to compare with FPI and HPCA densities), EPD/FPI/HPCA continuity of particle spectra, **V**(e-i) x **B** values compared to **E**, and others. This activity greatly enhances the unparalleled accuracy, which MMS provides to studies of space plasma physics, in general, and reconnection specifically.

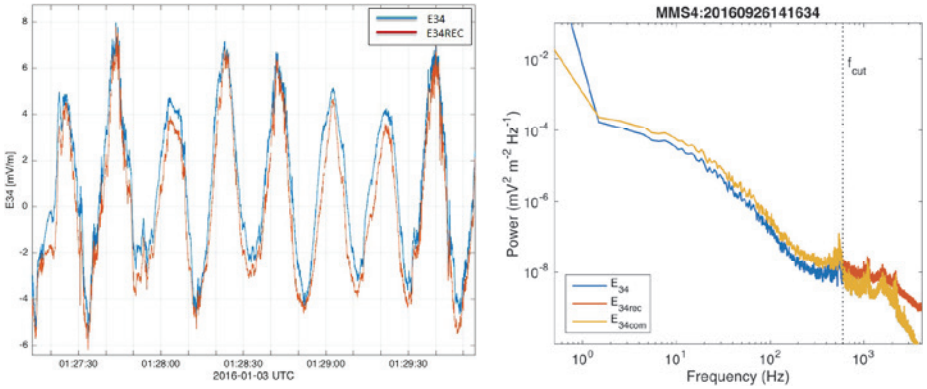

Figure 6.1-1. Comparison of (left) measured (blue) and reconstructed (orange) wave forms using data taken prior to the anomaly and (right) post-anomaly noise levels of the measured (blue), reconstructed (orange), and combined (yellow) products along the SDP3-4 axis.

6.2 Spacecraft System Status

All four MMS spacecraft are performing very well. Spacecraft bus performance requirements continue to be met and in some cases the actual performance far exceeds the engineering design. Two such examples are the Radio Frequency (RF) Communications subsystem and the Navigation subsystem. During spacecraft commissioning, the RF link margin between each spacecraft and the Deep Space Network (DSN) was observed to be more than 3 dB above design margins. This allowed the operations team to increase the maximum space-to-ground telemetry data rate from 2.5 to 5.0 Megabits per second (Mbps) during Phase 1 of the MMS mission. This, along with augmented DSN availability, has allowed the ground to capture more than double the amount of science data from the baseline design. The Navigation subsystem and the state-of-the-art design of the Navigator GPS receiver has provided navigation accuracy an order of magnitude better than expected, providing a direct benefit to MMS science in that the mean constellation spacing during mission Phase 1b could be reduced from 10 km to 7 km.

All spacecraft bus subsystems are performing reliably and within design requirements. There are no open subsystem or hardware risks and all hardware is expected to exceed its design lifetime, providing continued reliability for the MMS extended mission. The primary consumable for MMS is hydrazine propellant, used to maintain the mission orbit and attitude. Flight Dynamics Operations Area (FDOA) delta-v analysis shows that MMS can complete a 5-year extended mission with propellant reserve and the predicted Earth reentry will be around October 2036 (roughly 21.6 years after launch) which meets NASA's 25-year reentry requirement.

There have been few on-orbit anomalies during MMS Phase 1. Of particular note is that the Accelerometer Measurement System (AMS) on each spacecraft indicates that each spacecraft experiences an impact from a small micrometeoroid or space debris particle on nearly every orbit. This impact rate is no different from other spacecraft and the MMS structural design and orbital debris shields have mitigated any significant adverse effects from most of the impacts, with two exceptions. On February 2, 2016 a suspected micrometeoroid impact damaged one of four parallel shunt resistors on the bottom deck of MMS4. The Power and Thermal subsystem teams analyzed the post-impact telemetry data and concluded that the change in spacecraft performance was small and of no concern. On June 12, 2016 a suspected micrometeoroid damaged the MMS4 SDP4 bias channel wire (see §6.1.2) .

The Mission Director tracks all risks to the MMS mission using standard NASA risk management tools. The Continuous Risk Management (CRM) methodology is used to identify, analyze, plan, track, and control all mission risks. Operational mitigation techniques have been applied to maximize the likelihood that all four MMS observatories will continue to operate reliably during the MMS primary science mission and through the extended mission phase.

6.3 Mission Operations Status

The MMS Payload Operations Center (POC), located at LASP in Boulder, Colorado, operates the MMS Instrument Suites (ISs) in coordination with instrument teams. POC functions include routine planning and scheduling, command generation and uplink via the Mission Operations Center (MOC), health and safety assessment, contingency response, onboard and ground-based data management, and dissemination of data.

The multi-mission Flight Operations Team (FOT) at LASP staffs the POC and coordinates all IS operations activities on a daily basis. The MOC at Goddard Space Flight Center (GSFC) performs all MMS spacecraft bus operations. The MOC FOT provides mission planning, real-time pass operations, systems and networks administration, IT security, observatory data trending, and systems engineering support.

All MMS telemetry data (spacecraft and instrument housekeeping and science, in real-time and post-pass) are captured by the MOC and are relayed, as they are received, to the POC using a high reliability private operational network. In addition to telemetry data transfers ancillary data are also provided by the FDOA to the POC via the MOC interface. These data include predicted and definitive orbit ephemerides, spin axis attitude, spin rate and phase angle, as well as maneuver history information. The POC also provides a real-time flow of data to the instrument teams to support commanding activities.

All Level 0 telemetry data and Level 1 housekeeping data are managed in a database system at the POC, which currently contain approximately 30 terabytes (TB) of data, and is directly accessible by instrument teams and FOT staff within 60 minutes of a contact. Over 99% of the data collected onboard and requested for downlink has been successfully

captured on the ground and delivered to the instrument teams.

The MMS mission utilizes the DSN, TDRS and USN networks via standard NASA services to typically provide one DSN contact and 2-3 TDRS/USN contacts per 24 hours.

Over the course of an orbit, the MMS instruments perform a highly orchestrated sequence of operational and observational activities to maximize the science data return and quality from the MMS observatories. Each MMS orbit is separated predominantly according to science and non-science (e.g., calibration) priorities. Science data collection occurs while the spacecraft are in defined Regions of Interest (ROI), whereas the other portions of the orbit are used chiefly for calibration and maintenance activities. The planning process and rules-based scheduling system have been optimized over the course of the nominal mission and are operating with high efficiency.

Onboard burst data management is a key function performed by the POC, requiring ground-based assessment of onboard data and selection. To facilitate downlink of the optimal science data, the POC uses downlinked data to generate a set of default burst data selections, and makes these available to the science team via a Scientist-in-the-Loop (SITL) interface operated by the SDC. This interface enables the designated scientist to revise/improve the data selections, which are then submitted back to the POC, processed, checked, and used to produce a revised downlink plan. This system is working exceedingly well at maximizing the downlink of the highest value science data.

The current mission operations scenario is excellently suited to meet the future needs of the MMS mission in the extended mission phase.

7.0 Budget

The primary teaming arrangement for MMS is between GSFC, as the Project management organization, and Southwest Research Institute (SwRI). During Phase E, GSFC is responsible for overall project management, including grant administration, project science support, and mission operations. SwRI is responsible under contract to GSFC for leading the Solving Magnetospheric Acceleration, Reconnection, and Turbulence (SMART) science investigation, the elements of which include scientific research and publication, theory and modeling, science and payload operations, and data processing and analysis. The Project and SMART management teams have kept MMS spending within the Phase E budget constraints during the mission's remarkably successful first phase of science operations, which began on 1 September 2015. No changes are planned to the existing MMS management structure in the extended mission.

Two budget spreadsheets using constant FY17$ are attached. The first details the in-guideline MMS budget covering fiscal years 2018-2023; the second details an over-guideline budget for the same period. The in-guide budget assumes that operations end on 31 August 2017, with FY2018-FY22 budgeted only for declining data analysis, archival, and closeout efforts. The proposed over-guideline budget supports continued payload and mission operations and scientific research through FY23 and does not include a final closeout year.

MMS-SMART Budget. SMART funding supports project activities at SwRI and several subcontractor institutions as well as government contributions to SMART overseen by SwRI at GSFC, MSFC, and LANL. During Phase E, SwRI-SMART funding accounts for ~72% of the overall SMART budget, while the funding for the government side of SMART amounts to ~28% of the total budget. This apportionment is preserved in the budget for the extended mission.

We are proposing a robust over-guideline SMART budget that is based on the full SMART budget for Phase E ($55M), which includes unspent FY15 funds forwarded into Phase E ($7.5M). This budget will support continued operations and scientific research at levels comparable to those of the highly successful first phase of the mission and make it possible to realize the full promise of this unique mission. With its four spacecraft and 100 instruments, which enable a temporal and spatial resolution far exceeding that ever before achieved in space, MMS is a high-precision laboratory instrument of heretofore unimaginable capabilities. Limited fuel reserves render it essential to optimize scientific return enabled by the tight tetrahedral formation, an opportunity that will not occur again in the foreseeable future. Experience in the prime mission shows that fine-tuning of the MMS "microscope"—e.g., by adjusting spacecraft distances or by changing energy ranges, as was done in Phase 1b in response to lessons learned in Phase 1a—must be guided by the most recent scientific insights. Neither routine operations nor automated algorithms can serve as sub-

stitutes. Concurrent scientific analysis is therefore essential to maximize the scientific value of MMS-produced data sets, not only for the short term, but for long-term research utility. It is for this reason that we are asking for full science funding during the extended mission. Roughly 53% of the proposed SMART budget is to support instrument and science operations (i.e., obtaining, validating, calibrating, and archiving the data); the remaining 47% supports scientific research, including the addition of former members of the Interdisciplinary Scientist (IDS) teams to the SMART science team.

Budget for GSFC Management and Mission Operations. MMS Project Science and Mission Operations funding has supported activities at GSFC within the Heliophysics Science Division (HSD), at two IDS PI Institutions, the Space Sciences Mission Operations (SSMO) Project office, and the Mission Validation and Operations Branch, including diverse contracted services. During Phase E, Project Science and SSMO funding accounts for ~28% of the total mission budget, and this is roughly preserved in the proposed extended mission budget. Originally planned to end on 31 August 2017, MMS mission operations are proposed to continue through FY2023 in parallel with continued data analysis and archival.

We are proposing a robust extended mission operations budget that is based on experience with MMS tetrahedral formation flying operations during Phase E. These operations were, as expected, very challenging in terms of the number and frequency of maneuvers required to maintain the four spacecraft in scientifically optimal orbits. Thanks to the high precision of MMS' pioneering use of high altitude GPS positioning, outside the GPS constellation, the SSMO team was able to operate the spacecraft with mean separations as close as 7 km, which proved essential to fully resolve the electron physics of reconnection in Phase 1b.

MMS will continue to fly in tetrahedral formation at least through October 2021. Due to the significant margin carried in the propellant budget prior to execution of the fuel-intensive apogee raise campaign, which will be completed in early April 2017, it is likely that the tetrahedral formation can be maintained significantly longer. To ensure that the budget is not the limiting factor determining when MMS transitions from a formation to a "string of pearls" (requiring no formation maintenance), we have proposed a budget consistent with maintaining a formation for the full 5-year extended mission horizon. If the fuel limits the formation flying duration, we can adjust our operations cost downward to be consistent with the relaxation of formation keeping requirements. We will have better confidence in the fuel budget remaining for extended mission after the execution of the apogee raise campaign, so it will be available by time of the Senior Review panel briefing in April. Assuming that once formation flying is complete MMS will transition into a "string of pearls" with no or minimal requirements for maintaining inter-spacecraft range, operational simplifications can be made, resulting operational staffing reductions with a net savings of $687K per year to the mission operations cost.

8.0 References

Since the start of the prime mission, MMS observations and the results of related theory and modeling studies have been reported in over 300 articles and conference presentations.

Lists of MMS publications and conference presentations can be accessed at: https://lasp.colorado.edu/mms/sdc/

MMS papers in the special section of Geophysical Research Letters can be accessed here: http://agupubs.onlinelibrary.wiley.com/hub/issue/10.1002/(ISSN)1944-8007.NASAMMS1/

The "MMS Book," Space Science Reviews, 199 (1-4), March 2016, can be accessed here: http://link.springer.com/journal/11214/199/1/page/1

Anderson, B. J., et al. 2016, *GeoRL*, 43(12), 5988, doi:10.1002/2016GL069577.

Andre, M., et al. 2016, *GeoRL*, 43(13), 6705, doi:10.1002/2016GL069665.

Archer, M. O., et al. 2015, *P&SS*, 106, 56, doi: 10.1016/j.pss.2014.11.026.

Baker, D. N., et al. 2016, *GeoRL*, 43(12), 6051, doi:10.1002/2016GL069643.

Bessho, N., et al. 2016, *GeoRL*, 43(5), 1828, doi:10.1002/2016GL067886.

Birn, J., et al. 2009, *JGRA*, 114(A9), A00D03, doi:10.1029/2008JA014015.

Birn, J., et al. 2011, *JGRA*, 116(A1), A01210, doi:10.1029/2010JA016083.

Birn, J., et al. 2015, *EP&S*, 67, 110, doi: 10.1186/s40623-015-0282-3.

Breuillard, H., et al. 2016, *GeoRL*, 43(14), 7279, doi:10.1002/2016GL069188.

Burch, J. L., et al. 2016, *Sci*, 352(6290), aaf2939, doi:10.1126/science.aaf2939.
Burch, J. L. and Phan, T. D. 2016, *GeoRL*, 43(16), 8327, doi:10.1002/2016GL069787.
Chen, L.-J., et al. 2016a, *GeoRL*, 43(12), 6036, doi:10.1002/2016GL069215.
Chen, L.-J., et al. 2016b, *GeoRL*, 43(6), 2405, doi:10.1002/2016GL068243.
Cohen, I. J., et al. 2016, *GeoRL*, 43(12), 5960, doi:10.1002/2016GL068689.
Collier M. R., et al. 2003, Solar Wind 10 Conf. Proc., ed. M. Velli, R. Bruno, F. Malara (Pisa, Italy:AIP), 679(1), 790, doi:10.1063/1.1618711.
Cowley, S. W. H. and Owen, C. J. 1989, *P&SS*, 37(11), 1461, doi:10.1016/0032-0633(89)90116-5.
Doss, C. E., et al. 2015, *JGRA*, 120(9), 7748, doi: 10.1002/2015JA021489.
Drake, J. F., et al. 2006, *Natur,* 443, 553, doi:10.1038/nature05116.
Dubyagin, S., et al. 2011, *GeoRL*, 38(8), L08102, doi:10.1029/2011GL047016.
Eastwood, J. P., et al. 2016, *GeoRL*, 43(10), 4716, doi:10.1002/2016GL068747.
Eastwood, J. P., et al. 2013, *PhRvL*, 110(22), 225001, doi: https://doi.org/10.1103/PhysRevLett.110.225001.
Eastwood, J.P., et al. 2005, *SSRv*, 118, 41, doi:10.1007/s11214-005-3824-3.
Eastwood, J. P., et al. 2009, *PhRvL*, 102(3), 035001, doi:10.1103/PhysRevLett.102.035001.
Egedal, J., et al. 2008, *JGRA*, 113(A12), A12207, doi: 10.1029/2008JA013520.
Ergun, R. E., et al. 2016a, *PhRvL*, 116(23), 235102, doi:10.1103/PhysRevLett.116.235102.
Ergun, R. E., et al. 2016b, *GeoRL*, 43(11), 5626, doi:10.1002/2016GL068992.
Eriksson S., et al. 2016, *GeoRL*, 43 (11), 5606, doi:10.1002/2016GL068783.
Farrugia, C. J., et al. 2016, *GeoRL*, 43(12), 6070, doi:10.1002/2016GL068758.
Fennell, J. F., et al. 2016, *GeoRL*, 43(12), 6078, doi:10.1002/2016GL069207.
Fuselier, S. A., et al. 2016, *GeoRL*, 43(4), 1435, doi:10.1002/2015GL067358.
Gershman, D. J., et al. 2016, *GeoRL*, 43(9), 4112, doi:10.1002/2016GL068545.
Ghavamian, P., et al. 2013, *SSRv*, 178(2), 633, doi:10.1007/s11214-013-9999-0.
Gomez, R. G., et al. 2016, *GeoRL*, 43(18), 9374, doi: 10.1002/2016GL069692.
Gosling, J. T., et al. 2005, *JGRA*, Volume 110(A1), A01107, doi: 10.1029/2004JA010809.
Goodrich, K. A., et al. 2016, GeoRL, 43(12), 5953, doi:10.1002/2016GL069157.
Graham, D. B., et al. 2016, *GeoRL*, 43(10), 4691, doi:10.1002/2016GL068613.
Haggerty, C. C., et al. 2015, *GeoRL*, 42(22), 9657, doi: 10.1002/2015GL065961.
Hartinger, M. D., et al. 2013, *JGRA*, 118(1), 299, doi:10.1029/2012JA018349.
Hasegawa, H., et al. 2016, *GeoRL*, 43(10), 4755, doi:10.1002/2016GL069225.
Hasegawa H., et al. 2004, *Natur*, 430(7001), 755, doi:10.1038/nature02799.
Hesse, M., et al. 2016, *GeoRL*, 43(6), 2359, doi:10.1002/2016GL068373.
Hesse, M., et al. 2014, *GeoRL*, 41(24), 8673, doi:10.1002/2014GL061586.
Hoshino, M., et al. 1998, *JGRA*, 103(A3), 4509, doi:10.1029/97JA01785.
Huang, S. Y., et al. 2016, *GeoRL*, 43(15), 7850, doi:10.1002/2016GL070033.
Hwang, K.-J., et al. 2016, GeoRL, 43(18), 9434, doi:10.1002/2016GL070934.
Jaynes, A. N., et al. 2016, *GeoRL*, 43(14), 7356, doi:10.1002/2016GL069206.
Johlander, A., et al. 2016, *PhRvL*, 117(16), 165101, doi:10.1103/PhysRevLett.117.165101.
Khotyaintsev, Y. V., et al. 2016, *GeoRL*, 43(11), 5571, doi:10.1002/2016GL069064.
Kitamura, N., et al. 2016, *GeoRL*, 43(11), 5581, doi:10.1002/2016GL069095.
Lavraud, B., et al. 2016, *GeoRL*, 43(7), 3042, doi:10.1002/2016GL068359.
Le, G., et al. 2016, *GeoRL*, 43(6), 2396, doi:10.1002/2016GL068257.
Le Contel, O., et al. 2016a, *SSRv*, 199(1), 257, doi:10.1007/s11214-014-0096-9.
Le Contel, O., et al. 2016b, *GeoRL*, 43(12), 5943, doi:10.1002/2016GL068968.
Lee, S. H., et al. 2016, *GeoRL*, 43(14), 7338, doi:10.1002/2016GL069840.
Li, W., et al. 2016, *GeoRL*, 43(11), 5635, doi:10.1002/2016GL069192.
Liu, Y.-H., et al. 2014, JGRA, 119(12), 9773, doi:10.1002/2014JA020492.
Ma, X., et al. 2014, *JGRA*, 119(2), 808, doi: 10.1002/2013JA019225.
Matsui, H., et al. 2016, *GeoRL*, 43(18), 9397, doi:10.1002/2016GL070677.
Mauk, B. H., et al. 2016, *GeoRL*, 43(9), 4081-4088, doi:10.1002/2016GL068856.

Mozer, F. S., et al. 2016, *PhRvL*, 116(14), 145101, doi:10.1103/PhysRevLett.116.145101.
Nagai, T., et al. (2016), *GeoRL*, 43(12), 6028, doi:10.1002/2016GL069085.
Nagai, T., et al. 2015, *JGRA*, 120(10), 8762, doi: 10.1002/2015JA021606
Nakamura, R., et al. 2016, *GeoRL*, 43(10), 4841, doi:10.1002/2016GL068768.
Nakamura, R., et al. 2002, *GeoRL*, 29(20), 3-1, doi:10.1029/2002GL015763.
Nakamura, R., et al. 2004, *GeoRL*, 31(9), L09804, 10.1029/2004GL019558.
Narita, Y., et al. 2016, *GeoRL*, 43(10), 4774, doi:10.1002/2016GL069035.
Norgren, C., et al. 2016, *GeoRL*, 43(13), 6724, doi:10.1002/2016GL069205.
Nykyri, K. and Otto, A. 2001, *GeoRL*, 28 (18), 3565, doi: 10.1029/2001GL013239.
Oieroset, M., et al. 2016, *GeoRL*, 43(11), 5536, doi:10.1002/2016GL069166.
Oka, M., et al. 2010, *ApJ*, 714(1), 915, doi: 10.1088/0004-637X/714/1/915.
Oka, M., et al. 2016, *JGRA*, 121(3), 1955, doi: 10.1002/2015JA022040.
Petrinec, S. M., et al. 2016, *GeoRL*, 43(12), 5997, doi:10.1002/2016GL069626.
Phan, T. D., et al. 2016, *GeoRL*, 43(12), 6060, doi:10.1002/2016GL069212.
Phan, T. D., et al. 2013, *GeoRL*, 40(17), 4475, doi:10.1002/grl.50917.
Phan, T. D., et al. 2014, *GeoRL*, 41(20), 7002, doi:10.1002/2014GL061547.
Phan, T. D., et al. 2007, *GeoRL*, 34(14), L14104, doi:10.1029/2007GL030343.
Plaschke, F., et al. 2013, *AnnGeo*, 31(10), 1877, doi:10.5194/angeo-31-1877-2013.
Price, L., M., et al. 2016, *GeoRL*, 43(12), 6020, doi:10.1002/2016GL069578.
Pritchett, P. L., and Coroniti, F. V. 2013, *JGRA*, 118(1), 146, doi:10.1029/2012JA018143.
Reiff, P. H., et al. 2016, *GeoRL*, 43(14), 7311, doi:10.1002/2016GL069154.
Retinò, A., et al. 2007, *NatPh*, 3(4), 236, doi:10.1038/nphys574.
Runov, A., et al. 2012, *JGRA*, 117(A5), A05230, doi:10.1029/2011JA017361.
Schmid, D., et al. 2016, *GeoRL*, 43(12), 6012, doi:10.1002/2016GL069520.
Shay, M. A., et al. 2016, *GeoRL*, 43(9), 4145, doi:10.1002/2016GL069034.
Shepherd, L. S., and P. A. Cassak 2012, JGRA, 117(A10), A10101, doi:10.1029/2012JA017867.
Sibeck, D. G., et al. 2002, *JGRA*, 107(A10), SMP 4-1, doi:10.1029/2001JA007539.
Stawarz, J. E. 2016, Thesis (Ph.D.)-Univ. of Colorado-Boulder, Dissertation Abstracts International, 77-10(E), B, Pub Number: AAT 10108761, ISBN: 9781339720968.
Sundkvist, D., et al. 2007, *PhRvL*, 99(2), 025004, doi:10.1103/PhysRevLett.99.025004.
Torbert, R. B., et al. (2016), *GeoRL*, 43(12), 5918, doi:10.1002/2016GL069553.
Trattner, K. J., et al. 2016, *GeoRL*, 43(10), 4673, doi:10.1002/2016GL068554.
Turner, D. L., et al. 2016, *GeoRL*, 43(15), 7785, doi:10.1002/2016GL069691.
Turner, D. L., et al. 2013, *JGRA*, 118(4), 1552, doi:10.1002/jgra.50198.
Vernisse, Y., et al. 2016, *JGRA*, 121(10), 9926, doi:10.1002/2016JA023051.
Walker, S. N., et al. 2004, *AnnGeo*, 22(7), 2291, doi:10.5194/angeo-22-2291-2004.
Wang, S., et al. 2016a, *GeoRL*, 43(15), 7831, doi:10.1002/2016GL069842.
Wang, S., et al. 2016b, *GeoRL*, 43(10), 4850, doi:10.1002/2016GL069406.
Westlake, J. H., et al. 2016, *GeoRL*, 43(18), 9453, doi:10.1002/2016GL070189.
Wilder, F. D., et al. 2016a, *GeoRL*, 43(12), 5909, doi:10.1002/2016GL069473.
Wilder, F. D., et al. 2016b, *GeoRL*, 43(17), 8859, doi:10.1002/2016GL070404.
Wilder, F. D., et al. 2014, *JGRA*, 119(12), 9643, doi:10.1002/2014JA020453.
Wilson III, L. B. et al. 2014, *JGRA*, 119(8), 6475, doi: 10.1002/2014JA019930.
Wilson III, L. B. et al. 2013, *JGRA*, 118(3), 957, doi:10.1029/2012JA018186.
Wilson III, L. B. et al. 2016, *PhRvL*, 117(21), 215101, doi:10.1103/PhysRevLett.117.215101.
Wolf, R. A., et al. 2006, *JGRA*, 111(A12), A12218, doi:10.1029/2006JA012010.
Wolf, R.A., et al. 2009, *JGRA*, 114(A9), A00D05, doi:10.1029/2009JA014044.
Yordanova, E., et al. 2016, *GeoRL*, 43(12), 5969, doi:10.1002/2016GL069191.
Zhou, M., et al. 2016, *GeoRL*, 43(10), 4808, doi:10.1002/2016GL069010.

Appendix A: MMS Mission Archive Plan (MAP)

1 Introduction / Purpose

The purpose of this Mission Archive Plan (MAP) is to establish traceability for the MMS data systems to ultimately result in the permanent, long-term archival of the MMS science data in Space Physics Data Facility (SPDF), which is the designated long-term NASA archive facility. This document will present a plan that is focused on the data and metadata at the end of the mission, characterize the current status of the science data, and will outline a plan for finalizing the MMS Final Archive once the mission terminates. The plans outlined herein are intended to be entirely consistent with the NASA Heliophysics Science Data Management Policy. Any discrepancy is not the intent of the MMS project. It is anticipated that this plan will be updated, as needed, at each senior review to ensure that MMS archiving plans are consistent with mission status and future changes in NASA requirements or policies.

2 MMS Archive Plan Overview

With this MAP, the MMS project communicates a definitive vision towards completing the final mission archive and lays the foundation for future tasks with this end goal in mind. Although this MAP establishes formally, for the first time, the detailed archive plans for the mission, the project has, in fact, been proactively working towards a final archive since its very inception. With the original writing of the Project Data Management Plan (PDMP) in Phase B, through the construction and operation of the MMS ground data system to-date, the MMS project has been establishing the basis for an ultimately smooth transition to a long-term archive. Data products are produced in a centralized and highly coordinated fashion, and managed centrally within the project to established standards. Furthermore, the MMS

project has worked closely with personnel at the designated long-term archive facility, the NASA Space Physics Data Facility (SPDF), and has already been delivering MMS data to the SPDF for archiving on a routine basis. After operations terminate, the MMS project will complete the delivery of all remaining MMS data: Level-0, calibration data, software, additional data documentation, and other ancillary information to the SPDF.

3 The MMS Data System

The current data system for MMS consists of the Mission Operations Center (MOC), the Science Operations Center (SOC) consisting of the Payload Operations Center (POC) and the Science Data Center (SDC), Instrument Team Facilities (ITFs), and the SPDF. Each of these elements and/or institutions provides an essential ingredient to the production, timely availability, and archival of quality MMS science data products. The MMS SOC manages science operations, instrument operations, and selection, downlink, generation, management, distribution, and archiving of MMS science data sets, and consists of the POC and the SDC. The POC is responsible for all instrument operations, and the SDC is responsible for science data handling. Both are co-located at and managed by the Laboratory for Atmospheric and Space Physics (LASP) in Boulder, Colorado. MMS instrument teams conduct their operations through the POC, and utilize the Science Data Center (SDC) for data processing, data management, and distribution. The SOC provides a single mission data archive for housekeeping and science data, calibration data, ephemerides, attitude, and other ancillary data needed to support the scientific use and interpretation. All levels of data products reside at and are disseminated from the SDC. Documentation and metadata describing data products, algorithms, instrument calibrations, validation, and data quality are also managed at the SDC and maintained as part of the MMS data archive.

Figure 1 illustrates the role of the SOC in coordinating MMS operations and data handling efforts between the key components of the MMS ground segment.

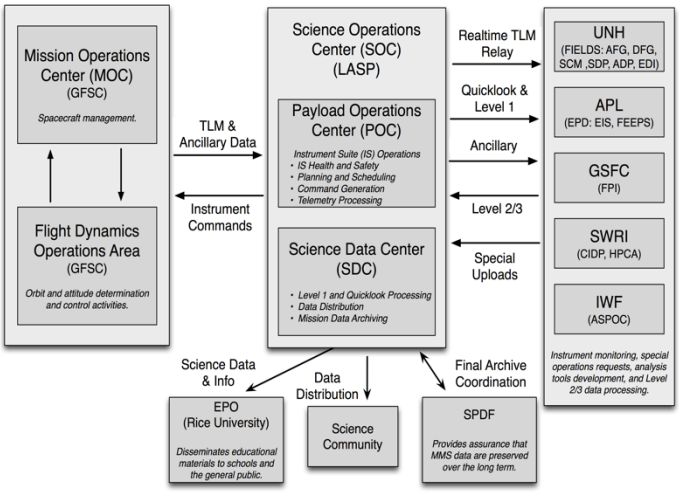

Figure 1. Overview of the MMS ground system showing the key elements and linkages between them. Major functions for each element are also shown where appropriate.

The SOC serves as the Mission Archive during the MMS mission, having responsibility for archiving all MMS mission data. Backup and recovery mechanisms are employed at the SOC and include contingency plans for ensuring a full recovery from catastrophic damage or failure. This includes offline and offsite backup of all irreplaceable information, including software, calibration data, and other system dependencies. Resources archived at the SOC include:

- Data – raw telemetry, calibration data, ephemerides, attitude and other ancillary data needed to support scientific use and interpretation of MMS data; all levels of science data products.
- Burst system metadata including burst quality values and data selections. These data may be useful for defining future data selection algorithms, and are thus included in the MMS archive.
- Metadata and documentation describing data products (e.g., in SPASE terms), algorithms, instrument calibrations, validation, and data quality; also, command and telemetry definition information, descriptions of spacecraft and instrument design and operations, status reports, and other information needed for use of MMS data.
- Software and analysis tools, including software used for generation of scientific data products and metadata, as well as tools used for accessing and displaying MMS science data.

During Phase 1 of the MMS mission, the SDC has taken in an average of 2 GB/day in the form of Level-0 and Ancillary data. These data are processed into Level-1 and Level-2 data products totaling approximately 200 GB/day and consisting of ~1500 files/day. The SOC has also collected and archived MMS data beginning with the pre-launch testing phase, principally telemetry data generated during ground testing and calibration activities. By the end of the prime MMS mission, more than 125 terabytes (TB) of science data is expected to be managed at the SDC. In addition to formal data management at the SDC and SPDF, a number of MMS team institutions "mirror" data for their own use, owing to the large data volumes and data access advantages of a local access node.

3.1 Ground System Data Flow

Responsibility for MMS data handling, including data processing and analysis activities, is a distributed function within the MMS mission, with each MMS instrument team having shared responsibility for generating and maintaining the MMS data during the active mission. Initial data capture occurs at the MOC. During ground station contacts, real-time telemetry data are relayed from the MOC to the POC. Following each ground station contact, the MOC provides the POC with recorded telemetry frames containing instrument and spacecraft data, and status and ancillary information. The POC performs Level-0 processing on these data, and makes these Level-0 data available for download by the MMS instrument teams. Level-0 data are then processed at the POC to form Level-1 *engineering* data products, which are used to monitor state-of-health and to support operations. Level-1 *science* data products are produced at the SDC and used to support Scientist-in-the-Loop (SITL) decision-making and are available within 1 hour of telemetry receipt. QuickLook science data products are created at the SDC to provide a preliminary view of MMS science measurements and are openly accessible to the science community via the Internet within 24 hours of ground receipt.

The SDC makes available telemetry and ancillary data to the instrument teams for Level-2 data processing. Each instrument team generates Level-2 data products based on current calibration factors and delivers these products within 30 days to the SDC for distribution and archival. Most instruments perform their processing in a hosted fashion within the SDC itself, streamlining this processing pipeline operation. However, some data sets are generated at instrument team institutions and delivered to the SDC. Development and maintenance of science processing software, data validation, and calibrations are the responsibility of each instrument team, with the SDC executing the provided software in a controlled production environment.

Updates to calibrations, algorithms, and/or processing software occur regularly, resulting in appropriate production system updates followed by reprocessing of science data products. Systems at the SDC and instrument team locations, where applicable, are designed to handle these periodic version changes and reprocessing activities. Publicly available software tools and documentation are updated as needed.

The SDC maintains an active archive of all MMS data levels, and provides direct access to the MMS science team and science community. Similarly, data products are transferred regularly to the SPDF for long-term archival and complimentary science community access. The SPDF uses the same interfaces to access the MMS data as do the MMS instrument teams themselves.

4 Summary of MMS Science Instrumentation

While the details of the MMS suite of instruments are fully described in other project documents and published journal articles, the following information briefly summarizes the instruments and their measurements to support the descriptions that follow in this document. The MMS Instrument Suite (IS) consists of the following complement of instruments:

The FIELDS investigation includes a sensor suite consisting of two axial and four spin-plane double-probe electric-field sensors (ADP and SDP), two flux-gate magnetometers (AFG and DFG), a search-coil magnetometer (SCM), and two electron drift instrument (EDI) per MMS spacecraft. These instruments measure the DC magnetic field with a resolution of 10 ms, the DC electric field with a resolution of 1 ms, electric plasma waves to 100 kHz, and magnetic plasma waves to 6 kHz.

The Energetic Particle Detector (EPD) includes an Energetic Ion Spectrometer (EIS) and two all-sky particle samplers called the Fly's Eye Energetic Particle Sensor (FEEPS) per MMS spacecraft. These instruments measure the energy-angle distribution and composition of ions (20 to 500 keV) at a time resolution of < 30 seconds, the energy-angle distribution of total ions (45 – 500 keV) at a time resolution of < 10 seconds, and the coarse and fine energy-angle distribution of energetic electrons (25 – 500 keV) at time resolutions of < 0.5 and < 10 seconds, respectively.

The Fast Plasma Instrument (FPI) includes four dual electron spectrometers (DES) and four dual ion spectrometers (DIS) per spacecraft. When the data from the two sets of four dual-spectrometers are combined, FPI is able to provide the velocity-space distribution of electrons from 10 eV to 30 keV and ions from 10 eV to 30 keV with a time resolution of 30 ms, and 150 ms, respectively.

The Hot Plasma Composition Analyzer (HPCA) measures the composition-resolved velocity-space distribution of ions from 1 eV to 40 keV with time resolution of 10 – 15 seconds. There is one HPCA per MMS spacecraft.

The Active Spacecraft Potential Control (ASPOC) generates beams of indium ions to limit positive spacecraft potentials within +4V in order to improve the measurements obtained by FPI, HPCA, ADP, and SDP. There are two ASPOC per MMS spacecraft.

5 MMS Data Products

The MMS project produces a large complement of data products, which are described below. All scientific data products that are made publicly available or interchanged between institutions at intermediate levels of processing use the standard Common Data Format (CDF).

5.1 Data Level Descriptions

The MMS project produces, manages, and disseminates multiple categories of data, each of which has a specifically defined level of refinement. MMS uses the data level definitions indicated in Table 1.

Data Level	Brief Description
Raw	Raw telemetry data as received at the ground receiving station or ground test Ground Support Equipment (GSE), organized by contacts or ground test. Data sets may overlap and/or contain communication artifacts.
Level-0	Reconstructed, unprocessed instrument and spacecraft data in the form of CCSDS packets with communications artifacts and duplicate data removed.
Level-1A	Fully decommutated and uncalibrated raw data at full resolution; time-referenced; "extracted telemetry items"
Level-1B	Level-1A to which engineering (e.g., simple polynomial) calibrations have been applied; data have been annotated with ancillary information (e.g., ephemeris, attitude) and initial instrument science calibrations applied.
QuickLook	Scientific data products generated using simplified science processing algorithms and/or with provisional calibrations. Intended to provide basic scientific insight as quickly as possible. In many cases, Level-1B products serve as QuickLook data.
Level-2	Level-1 data that have been processed to physical units and/or derived geophysical parameters by combining calibration, ancillary, and other data. These data represent the lowest level of research grade scientific data, and exist at the same time and/or spatial resolution as Level-1 data.
Level-3	Science data that have been resampled spatially and/or temporally and/or may have been combined with measurements from other MMS spacecraft or instruments to produce a merged data set.

Table 1: MMS Data Level Definitions. Each instrument team bases their data products on this set of guiding definitions.

5.2 Level-1 Data

Level-1 data products are uncalibrated or partially calibrated only and thus do not provide scientific value to the science community. As such, these data products are not made accessible through public data interfaces, but are included in the MMS data archive. They are used extensively, however, in facilitating the SITL process, serving as QuickLook, and are the building blocks for higher-level science products. Level-1 science data products are already being delivered to the SPDF for long-term archiving.

5.3 QuickLook Data

Generation of QuickLook data occur at the SDC within hours of receipt, and consist of graphical plots of selected scientific parameters. Plots are generated within 24 hours to provide rapid exploration of the data from individual instruments, high-value line plots and spectrograms, or in the form of summary plots that combine data from the entire instrument suite and provide a picture of the spacecraft environment (41 unique plots per day). The SDC produces these daily plots such that users may view the entire day at a glance, or zoom into features of interest at a higher temporal resolution.

In addition to providing rapid assessment of the data from each instrument, the QuickLook plots provide information regarding the current observation modes of the spacecraft. Indicators are included for where data is collected in the Fast versus Slow modes, as well as indicating where the highest resolution Burst segments have been downlinked. Because burst segments are subsequently downlinked based on their Figure-of-Merit over an extended period of time, the SDC regenerates the Quicklook plots after 30, 60, and 90 days to update for additional data availability.

QuickLook data/plots are likely to be a useful long-term browse products and are thus already being delivered to the SPDF for long-term archiving.

5.4 Level-2 Data

Level-2 data represent the lowest level of research grade scientific data and include metadata appropriate to aid in correct use. Current Level-2 data products are summarized below in Table 2. A detailed description of all MMS Level-2 data products, including file structures and naming conventions, is provided on the MMS SDC web site. Level-2 science data products are already being delivered to the SPDF for long-term archiving and to enhance ready community access to these data.

Inst.	# of Products	Description	Volume /day	Latency
ASPOC	1	• Ion beam energy • Current for each of the two ASPOCs • Sum of the currents from the two ASPOCs at 1 second time resolution	16 MB	<24 Hours
EPD	5	• Calibrated ion intensities as a function of mass species (H, He, O), energy, and look direction for the higher energy range (derived from time-of-flight x Energy) of the EIS sensor with viewing directions mapped to magnetic field direction and geophysical coordinates. • Calibrated ion intensities as a function of mass species (H, O), energy, and look direction for the lower energy range (derived from time-of-flight x Pulse Height) of the EIS sensor with viewing directions mapped to magnetic field direction and geophysical coordinates. • Calibrated (Intensity) electron data cubes: Intensity x Energy x Sector Elevation x Sector Longitude versus time, sampled 1/8 spin period combined for both heads with each sector mapped to a Geophysical-Coordinate look direction and magnetic field direction. • Calibrated (Intensity) electron data cubes: Intensity x Energy x Detector versus time, at the instrument sampling rate combined for both heads (18 detectors total) with each detector mapped to a Geophysical-Coordinate look direction and magnetic field direction.	3.4 GB	<30 Days
FPI	4	• Moments (density, velocity vector, temperature vector, pressure tensor, heat flux vector) • Velocity distributions (with spacecraft potential corrections) in 3D: supporting various slices, projections, or reductions (pitch angle, ecliptic, GSM equator, etc. portrayals).	31.3 GB	<30 Days
FIELDS	7	• 3-component B-field to 128 vectors/sec • E-Field vectors (AC and DC), spacecraft potential, and electric spectra in two frequency ranges • 3-component measurements of AC B-field, low-frequency magnetic spectra, and high speed B-field waveform. • Ambient electrons, electric field, and drift velocity measurements.	50.4 GB	<30 Days

Inst.	# of Products	Description	Volume /day	Latency
HPCA	2	• Calibrated and background-corrected energy flux for H+, He+, He++, and O+ ions • Velocity distribution functions of H+, He+, He++, and O+ ions derived from j(E). • Moments (density, velocity, temperature)	4.4 GB	<30 Days

Table 2: MMS Level-2 Science Data Products. Volumes are cumulative for all four observatories.

5.5 Level-3 Data

Level-3 data products extend beyond the original mission requirements and will include data and analysis results pertaining to specific encounters with the Electron Diffusion Region (EDR). Additional products will also be considered to enhance the understanding and usability of MMS data. Level-3 products and associated software will be archived at and made available from the SDC, and become part of the permanent MMS mission archive at the SPDF, delivered routinely as is currently done with Level-2 data. Specific products, when developed, will be listed in a future version of this document.

5.6 Magnetic Ephemerides

In partnership with the Los Alamos National Laboratory (LANL), Magnetic Ephemerides files are generated and delivered to the MMS SDC for archiving and dissemination, as summarized in Table 3. These files contain the Northern and Southern magnetic field line footprints of the spacecraft calculated by using a number of magnetic field models, along with the model magnetic field vector at each spacecraft, location and value of the minimum B-point, and loss cone size. In addition, the position and velocity of each spacecraft is provided in various coordinate systems (ECU, GSM, SM, GEO, GSM) along with the coordinate transformation quaternions, the position of the Sun and Moon, and eclipse flags.

Product Name	Magnetic Field Model	Resolution
EPHTS04D	TS04D, with dynamic model inputs	30 ms
EPHT89Q	T89Q, Kp = 2	30 ms
EPHT89D	T89D, Variable Kp	30 ms

Table 3: Magnetic Ephemerides Products

These ephemeris products are already being delivered to the SPDF for long-term archiving.

5.7 Spacecraft, Flight Dynamics, and Mission Data

Engineering and housekeeping data are stored within the mission archive at the SOC and will be provided to the SPDF for long-term archiving once the mission is terminated. Additionally, information about spacecraft events, including all products originating from the Flight Dynamics Operations Area (FDOA) are also stored at the SOC. A number of these products are actively served to the MMS team for use in data processing, as well as supporting instrument operations and health/safety analyses.

FDOA data products are already being delivered to the SPDF for long-term archiving. Spacecraft, engineering, and other mission data will be delivered to the SPDF for archiving at mission closeout.

5.8 Calibration Data

Calibration data are parameters and other information used as input to the data processing software to facilitate generation of usable science products. In many cases, these calibration data are delivered to the SDC to be used for science data processing, and are thus managed along with the associated science data products. In other cases, the calibration data remain at ITFs where selected processing functions

take place. In all cases, calibration data are produced and maintained by instrument teams, and will be delivered to the SPDF to become part of the MMS archive at mission closeout.

5.9 Data Processing Software

The software/algorithms used to generate the science data products is created and maintained by MMS instrument teams. In many cases, this software is delivered to the SDC for execution and is thus managed along with the respective science data. In other cases, software is resident at ITFs and used for data processing at those locations. In all cases, software in the form of source code will be formally delivered to the SPDF and become part of the MMS permanent archive as part of the mission closeout process following termination of operations.

5.10 Data Product File Formats

The MMS project uses the standard Common Data Format (CDF) for all publicly available scientific data products. This format is intended to be familiar and convenient for the scientific communities that the MMS program serves. The utilization of a common file format facilitates the use of MMS data in multi-mission science studies and allows the data to be readily used with existing user tools. CDF is used by several other NASA missions, including Cluster, THEMIS, and the Van Allen Probes, and is an actively supported product of NASA's SPDF.

5.11 Data Product Volumes

The MMS instrument suite produces a substantial volume of data on a daily basis. Level-2 data products alone account for more than 50 GB per day for all four observatories. Table 4 summarizes the total data volumes for each MMS investigation's data products, as managed by the SOC. For raw and Level-0 data, only the total volumes are shown, as all instruments' data are packaged together at these levels.

Instrument	Raw & L0 Volume	L1 & QL Volume	L2 Volume	Total
Fast Plasma Instrument		408	3845	4253
Hot Plasma Composition Analyzer		477	122	599
Fluxgate magnetometer - AFG		94	103	197
Fluxgate magnetometer - DFG		93	103	196
Search-coil magnetometer		884	457	1341
Axial double-probe and Spin-plane electric field instrument		1689	2593	4282
Electron-drift electric field instrument		319	134	453
Energetic Particle Detector		2	1	3
Active Spacecraft Potential Control		n/a	23	23
Magnetic Ephemeris		408	3845	4253
Total	3000	4062	7509	11571

Table 4: MMS data volume totals as of 11/1/2016 (GB, uncompressed, for each spacecraft. For totals, multiply by 4).

6 Data Access and Availability

The MMS ground data system is designed to fully enable timely availability of the simultaneous measurements from all four MMS spacecraft, and there are no proprietary periods associated with any of the MMS data products. The MMS SDC functions as an active online data center, from which all MMS science products of all levels are made available, as well as basic tools that aid in data access and analysis. All data products are freely available via the MMS SDC web site and via programmatic data services that the SDC provides. Science products that also currently reside on the SPDF are also made available presently through the SPDF data interfaces and analysis tools.

6.1 Science Data

The general science community is able to access MMS science data products via a publicly accessible interactive web site, which is maintained and hosted at the SDC. The SDC also makes data products available via RESTful "programmer level" or direct-access interfaces, which enables access by "power users" who already know what they want, automated processing and analysis systems at other institutions, as well as Virtual Observatories (VxOs). In addition, MMS data are currently made available through existing SPDF multi-mission data services such as CDAWeb and orbit services such as SSCWeb to further enable multi-mission science studies using MMS data and to more easily use data from other missions to establish the larger context for given MMS observations.

In order to most effectively index, store, and distribute the MMS data, documentation and metadata accompany the data products. Documentation and metadata support the Space Physics Archive Search and Exchange (SPASE) data model so that the SDC can readily provide access to the data through VxOs. The MMS team collaborates with applicable VxOs to ensure that MMS data are also accessible through these channels.

6.2 Ancillary Data

In addition to the science data files, the SDC provides access to a variety of ancillary data to assist in the analysis and interpretation of MMS data, including spacecraft ephemeris and attitude information, instrument operating parameters, version history notes, and other supporting information. The majority of this ancillary data is available through the same web based interfaces as the science data, with the exception of event data and Scientist-in-the-Loop reports, which are customized for these unique elements.

Spacecraft ephemerides, both predicted and definitive, are stored and made available in ASCII and SPICE formats to assist in the reconstruction of the MMS positions along with spacecraft attitude information and tetrahedron quality factors. The mission timeline, an XML formatted log of maneuvers, L-shell crossings, apogees, perigees, and downlinks, is also available.

The SDC maintains a searchable database of spacecraft events and parameters. Included in this database are all the selections, comments, and figure-of-merit classifications of burst data segments downlinked from the MMS spacecraft. These burst segments are the highest temporal and spatial resolution data for the MMS mission, so are of greatest interest to the majority of the heliospheric community. The selection database provides a convenient point of entry to the data for those not directly involved in the MMS mission.

6.3 Engineering Data

Spacecraft and instrument suite housekeeping/engineering data have minimal scientific value and may also be subject to export restrictions. Many of these data are only available to MMS team members and other designated individuals or organizations; however, effort is made to ensure that all housekeeping and engineering data that are necessary to support the use and interpretation of MMS science data are made publicly available from the SDC web site, along with the MMS science data products. All data are managed within the SOC and are considered part of the essential MMS archive.

6.4 Data Access and Analysis Tools

The SDC provides access to interfaces and software tools to allow basic display and manipulation of MMS science data, and also refers users to mature community-based tools that provide much more powerful analysis capabilities. These tools are made available to the science community via the SDC's data access website. The SDC makes this data publicly available primarily through web services that allow the user to search, list, and download the science and ancillary data files held at the SDC, either manually through their web browser or as part of an automated script. Additionally, the SDC website includes GUI interfaces to the web services to facilitate data exploration for users who prefer an interactive environment. MMS also continues to work closely with the SPDF to facilitate access through the SPDF's data services and in conjunction with data from other current missions and data sources.

The decision to base the Scientist-in-the-Loop, SITL, selection tools on the SPEDAS software suite has resulted in a comprehensive data access and plotting tool that is available to the heliophysics community. Through active development and updates, this IDL-based software package can directly access MMS data from the SDC, read the CDF files, and make data available for plotting or manipulation.

For users without access to IDL, many SPEDAS capabilities are also available using the IDL virtual machine architecture. In addition, the MMS project has worked with the developers of other community tools such as Autoplot to ensure that they can seamlessly provide data access. By working with the community to extend existing software capabilities, MMS has provided greater access through familiar tools without incurring the development costs of new software.

7 Documentation and Metadata Status

All science data produced by the MMS science team complies with metadata standards through ISTP compliant, self-describing CDF data files. Significant effort has been made to ensure that each CDF file contains the necessary information to allow analysis of the data, either through widely available plotting tools or through custom code produced by the user.

To fully understand and interpret the complex and interrelated data from the MMS mission, each instrument team has provided a Data Products Guide, available through the SDC website, in which the relevant details of each instrument are discussed. In some cases, this includes the construction of the instrument, its calibration, operational parameters, caveats related to the data, compression algorithms, and known issues. Efforts are made to keep these documents up to date as new characteristics are discovered during the mission, and a final set will be produced after the completion of routine operations.

Additional documentation exists in the form of Version Release Notes. Each data product produced by a MMS science team adheres to a standard data versioning convention, which is used to reflect changes in software, algorithms, calibrations, or data formats.

8 Mission, Resident, and Permanent Archives

As specified in the current Heliophysics Science Data Management Policy, the SPDF is designated as the long-term archive MMS. As noted previously, the MMS project has worked closely and enthusiastically with the SPDF in standards (i.e., use of the CDF data standard and ISTP/SPDF metadata standards) and in supplying all publicly-available MMS data to the SPDF immediately, both to further enhance community access, review and use of MMS data immediately, and to proactively ensure long-term archiving of MMS science data while the project and instrument teams are still fully active and involved.

Once routine operations ends, MMS will complete the archiving of the entire MMS data set at the SPDF, including all levels of data, processing and calibration software, calibration data, documentation, and metadata. While most of the MMS science data volume is already being delivered to the SPDF, these additional supporting products/software will become part of the permanent MMS data archive at the SPDF at mission closeout.

The MMS project believes that there may be value in maintaining a Resident Archive for a period of time after mission closeout, and will discuss this possibility with NASA at that time. A Resident Archive may provide additional benefit to the scientific community in maintaining interfaces and other support tailored to the MMS data set, although it is not necessary for completion of the final MMS archive.

Appendix B: MMS Acronym List

Acronym	Definition
AC	Alternating Current
ACE	Advanced Composition Explorer
ADP	Axial Double Probe
AFG	Analog Fluxgate
AGU	American Geophysical Union
AMS	Accelerometer Measurement System
ApJ	The Astrophysical Journal
ARTEMIS	Acceleration, Reconnection, Turbulence and Electrodynamics of the Moon's Interaction with the Sun
ASPOC	Active Spacecraft Potential
ASCII	American Standard Code for Information Interchange
BBF	bursty bulk flows
CCSDS	Consultative Committee for Space Data Systems
CDAWeb	Coordinated Data Analysis Web
CDF	Common Data Format
CME	Coronal Mass Ejection
CRM	Continuous Risk Management
DC	Direct Current
DES	Dual Electron Sensor
DF	distribution functions
DF	dipolarization fronts
DFB	dipolarized magnetic flux bundle
DFG	Digital Fluxgate
DIS	Dual Ion Sensor
DSCOVR	Deep Space Climate Observatory
DSN	Deep Space Network
EDI	Electron Drift Instrument
EDR	Electron Diffusion Region
EIS	Energetic Ion Spectrometer
EPD	Energetic Particle Detectors
EP&S	Earth, Planets and Space
ERG	Exploration of energization and Radiation in Geospace
FDOA	Flight Dynamics Operations Area
FEEPS	Flys Eye Energetic Particle Spectrometer
FIELDS	MMS suite of electric and magnetic field instruments
FOT	Flight Operations Team
FPI	Fast Plasma Intrument
FTE	Flux Transfer Events
FY	Fiscal Year
GB	gigabyte
GDU2	Gun-Detector Unit 2
GEO	geographic coordinate system
GOES	Geostationary Operational Environmental Satellite
GSFC	Goddard Space Flight Center
GPS	Global Positioning System
GSE	Geocentric Solar Ecliptic

Acronym	Definition
GSM	Geocentric Solar Magnetic
HPCA	Hot Plasma Composition Analyzer
HSD	Heliophysics Science Division
HSO	Heliophysics System Observatory
HV	High Voltage?
IBEX	Interstellar Boundary Explorer
ICME	Interplanetary Coronal Mass Ejection
IDL	Interactive Data Language
IDS	Interdisciplinary Scientist
IMF	Interplanetary Magnetic Field
ITF	Instrument Team Facilities
IS	Instrument Suites
IT	Information Technology
ISTP	International Solar Terrestrial Physics
KH	Kelvin-Helmholtz
KHI	Kelvin-Helmholtz instability
LHD	lower-hybrid drift
LANL	Los Alamos National Laboratory
LASP	Laboratory for Atmospheric and Space Physics
LT	Local Time
MAP	Mission Archive Map
MB	megabytes
Mbps	Megabits per second
MCP	Microchannel plate
MHD	magnetohydrodynamic
MMS	Magnetospheric Multiscale Mission
MOC	Mission Operations Center
MSFC	Marshall Space Flight Center
N/A	Not applicable
NASA	National Aeronautics and Space Administration
PDMP	Project Data Management Plan
PI	Principal Investigator
PIC	Particle in cell
POC	Payload Operations Center
PSBL	plasma sheet boundary layer
P&SS	Planetary and Space Science
PSG	Prioritized Science Goal
R_E	Earth radii
RF	Radio Frequency
ROI	Regions of Interest
SDC	Science Data Center
SMD	Science Mission Directorate
SDP	Spin-plane Double Probe
SITL	Scientist-in-the Loop
SM	solar magnetic
SOC	Science Operations Center
SOHO	Solar and Heliospheric Observatory

Acronym	Definition
SPASE	Space Physics Archive Search and Extract
SPDF	Space Physics Data Facility
SPEDAS	Space Environment Data Analysis System
TB	terabytes
SMART	Solving Magnetospheric Acceleration, Reconnection, and Turbulence
SSCWeb	Satellite Situation Center Web
SSMO	Space Sciences Mission Operations
STEREO	Solar Terrestrial Relations Observatory
SwRI	Southwest Research Institute
TDRS	Tracking and Data Relay Satellite
TDS	time domain structures
THEMIS	Time History of Events and Macroscale Interactions during Substorms Mission
TIFP	transient ion foreshock phenomena
TWINS	Two Wide-angle Imaging Neutral-atom Spectrometers
UCLA	University of California – Los Angeles
USN	Universal Space Network
VxOs	Virtual Observatories
XML	Extensible Markup Language